

Instituto Tecnológico y de Estudios Superiores de Monterrey
Campus Monterrey
School of Engineering and Sciences



Data-Driven Control of DC-DC Power Converters

A thesis presented by

Benjamín Alejandro Frías Araya

Submitted to the
School of Engineering and Sciences
in partial fulfillment of the requirements for the degree of

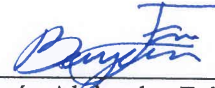
Master of Science
in
Engineering Science

May 2019

Declaration of Authorship

I, Benjamín Alejandro Frías Araya, declare that this thesis titled, “Data-Driven Control of DC-DC Power Converters” and the work presented in it are my own. I confirm that:

- This work was done wholly or mainly while in candidature for a research degree at this University.
- Where any part of this thesis has previously been submitted for a degree or any other qualification at this University or any other institution, this has been clearly stated.
- Where I have consulted the published work of others, this is always clearly attributed.
- Where I have quoted from the work of others, the source is always given. With the exception of such quotations, this thesis is entirely my own work.
- I have acknowledged all main sources of help.
- Where the thesis is based on work done by myself jointly with others, I have made clear exactly what was done by others and what I have contributed myself.



Benjamín Alejandro Frías Araya
Monterrey Nuevo León, May 22nd, 2019

©2019 by Benjamín Alejandro Frías Araya
All rights reserved

Dedication (in Spanish)

A mi familia, sin cuya ayuda esto simplemente no habría sido posible. Hoy, este logro es mío gracias a ustedes.

Acknowledgements (in Spanish)

Agradezco a mi mamá, Mary Araya, por darme el conocimiento, apoyo y cariño necesarios para sobrevivir mis primeros dos años fuera de casa, y por atender mis llamadas diarias aunque fueran inoportunas y sin propósito. Por visitarme sin fin de veces y traerme un pedacito de casa cuando tanto lo añoraba. *Gracias por todo, siempre.*

A mi papá, Benjamín Frías, por brindarme apoyo, sustento y cariño incondicional durante mis estudios de maestría, y por enseñarme que la tenacidad, valor e intrepidez resuelven problemas mejor que cualquier otra fórmula. *Gracias por todo, siempre.*

A mi hermana, Alejandra Frías, por enseñarme a poner mi propio bienestar mental sobre todas las cosas. *Gracias por darme consejos y enviarme emojis para mitigar mi estrés.*

A mi asesor, Jonathan Mayo, por mostrarme que ser buena onda y un prodigio en el área de estudio no son características mutuamente excluyentes. Por su paciencia y apoyo durante la elaboración de esta tesis, y por haber sembrado en mí una motivación por aprender. *Trabajar contigo ha sido una experiencia increíble; gracias por transmitir tu conocimiento siendo siempre claro e interesado por el aprendizaje ajeno.*

A mi comité de tesis, Omar Ruiz y Servando López, por aceptar la tarea de revisar este trabajo. Su apoyo en implementaciones, observaciones e ideas fueron clave en el desarrollo y mejora de mi proyecto de tesis.

A Luis y Ángel Bautista, por demostrarme que la amistad verdadera no conoce de fronteras. Por todas las horas de risas, videojuegos, discusiones y conversaciones desde lo más banales hasta lo más significativas. *Luis, el Pípila no fue real. Ángel, ahí te hablo cuando me haya encantado la película de Flight. Gracias a los dos por haber sido mis hermanos lejos de casa. Los llevo dentro siempre.*

A Enrique Soto, Angélica Orona, Marcela Herrera y Fabián Lugo, por haberme ayudado a mantener un equilibrio entre mi vida social y académica siendo excelentes amigos y personas. *Espero CEDES no se sienta tan vacío sin mis visitas repentinas. Gracias por estar ahí; los voy a extrañar mucho.*

A mis amigos tijuanenses por no hacerme extrañarlos tanto, y por ser la fuerza que a distancia me empujaba hacia adelante. *Nos vemos pronto; espero me reciban con tacos, pero de favor les suplico que tengan guacamole.*

Al Tecnológico de Monterrey por el apoyo otorgado con la beca de colegiatura, y a CONACYT por proveer manutención durante dos años. Este proyecto se llevó a cabo en tiempo y forma gracias, en gran parte, al sustento brindado por ambas organizaciones.

Finalmente, a Griselda Ruiz por regalar su tiempo para escucharme. *Gracias por contestar el teléfono ese día.*

Data-Driven Control of DC-DC Power Converters

by

Benjamín Alejandro Frías Araya

Abstract

In this thesis we develop a data-driven approach to the control design of power converters. We show that, given a set of measured data containing information about *variables of interest* (duty cycle as the input and inductor current/capacitor voltage as outputs) in the system, we can achieve asymptotic stability by solving a set of Lyapunov linear matrix inequalities (LMIs). This approach effectively addresses the issue of performance degradation in controllers operating over networks, i.e. feeding constant power loads (CPL) as opposed to their *standalone* design, i.e. with nominal resistive loads.

In order to do so, we study elements of behavioral system theory such as linear difference systems and quadratic difference forms; this allows for the creation of a framework compatible with higher-order discrete systems, which guarantees asymptotic stability in power converters both in standalone operation and with increased modeling complexity when interconnected to a network.

Moreover, given the fact that the aforementioned LMIs provide us with multiple stabilizing gain solutions, we develop an algorithm for the synthesis of a switching multi-controller framework which, given a *family of controllers*, endeavors to select the single best-performing set in order to improve the dynamic profile of a to-be-controlled system, e.g. a power converter.

Simulations and experimental results are provided as proof of concept, thus validating the theoretical material and illustrating the advantages of the proposed approaches.

Contents

Notation	ix
1 Introduction	1
1.1 Overview of problem and contributions	2
1.2 Objective of the thesis	5
1.3 Outline of the thesis	5
2 Continuous-time control of DC-DC converters	7
2.1 Preliminary background material	7
2.1.1 State space representations	7
2.1.2 Lyapunov stability theory	8
2.2 Modeling of DC-DC power converters	9
2.2.1 Large-signal modeling	9
2.2.2 Small-signal modeling: Approximate linearization	10
2.3 Control of DC-DC power converters	12
2.3.1 Linear control design	12
2.3.2 Commercial boost converter control: Gain tuning	13
2.4 Multi-controller system	14
2.5 Simulation Results	16
2.5.1 Open loop traditional boost converter	17
2.5.2 Linear control of boost converter	18
2.5.3 Multi-controller switching system	18
2.6 Conclusion	25
3 Behavioral system theory	27
3.1 Linear difference systems	27
3.2 Quadratic difference forms	28
3.3 Lyapunov stability criteria	29
3.4 Conclusion	31
4 Data-driven control of DC-DC converters	33
4.1 Data suitability: Hankel matrix criteria	33
4.2 Classification of variables	34
4.3 Persistency of excitation	34
4.4 Computation of coefficient matrices from data	35
4.5 Control design purely from data	37
4.6 Gain computation	39
4.7 Results	40

4.7.1	Control of DC-DC converter with nominal resistive load	40
4.7.2	Control of DC-DC converter with DC machine load	44
4.7.3	Experiment: Control of DC-DC converter with constant power load (CPL)	46
4.7.4	Data-driven multi-controller system	50
5	Conclusions and future work	55
A	MATLAB Codes	59
A.1	Continuous-time	59
A.1.1	Nonlinear model solver in open loop	59
A.1.2	Continuous-time control: Gain computation by Lyapunov LMI solving	61
A.1.3	Nonlinear model solver in closed loop with multi-controller function	62
A.2	Discrete-time	67
A.2.1	Data extractor: Importing data from .txt file to MATLAB and reducing its integration step	67
A.2.2	Hankel matrix builder from data set in time-series form: Lag 1 . .	68
A.2.3	Hankel matrix builder from data set in time-series form: Lag 2 . .	69
A.2.4	Discrete-time control: Gain computation by Lyapunov LMI solving (LDS of lag 1)	70
A.2.5	Discrete-time control: Gain computation by Lyapunov LMI solving (LDS of lag 2)	71
A.2.6	Linearized model solver in closed loop	73
	Bibliography	75

List of Figures

1.1	<i>Zooming</i> on DC-DC converter operating over a network for control purposes. . . .	3
1.2	Controller re-design process via data-driven approach.	4
1.3	General diagram of switching control [1].	5
2.1	Traditional boost converter topology.	9
2.2	Topologies induced by switching.	9
2.3	General feedback controller for a linearized converter.	12
2.4	Predefined feedback controller example.	13
2.5	Multi-controller operation.	16
2.6	Boost converter simulation results.	17
2.7	Controlled boost converter simulation results.	19
2.8	Algorithm for controller bank generation.	19
2.9	Stabilizing controller bank for $n = 40$	20
2.10	Multi-controller structure performance for $\epsilon = 0.1$	21
2.11	Multi-controller structure performance for $\epsilon = 0.01$ and different trajectory. . . .	22
2.12	Multi-controller structure performance for varying ϵ (0.3).	22
2.13	Multi-controller structure performance for varying ϵ (0.2).	23
2.14	Multi-controller structure performance for varying ϵ (0.01).	23
2.15	Multi-controller performance under abrupt changes in output resistance.	24
2.16	Multi-controller performance under abrupt changes in input voltage.	24
2.17	Multi-controller performance for trajectory following.	25
2.18	Changes in controller set index i for multi-controller system.	25
4.1	Algorithm for the computation of the coefficient matrix \tilde{R} from measurement data. . . .	36
4.2	General realization of a data-driven feedback controller in state space form. . . .	38
4.3	Predefined feedback controller example.	39
4.4	Varying input signal.	41
4.5	Boost converter with variable input used to gather data.	41
4.6	Unstable voltage response for data gathering.	42
4.7	Control circuit implemented in PSIM.	43
4.8	Circuit response to data-driven controller.	43
4.9	Disturbance rejection at time step $t = 0.4s$	43
4.10	Boost converter with DC machine load.	44
4.11	Unstable voltage response for data gathering in DC machine-loaded circuit. . . .	45
4.12	Controlled voltage of a Boost converter with DC machine load.	45
4.13	Controlled current in Boost converter.	46
4.14	Source and load converters and corresponding controllers.	47
4.15	Experimental setup.	48

4.16	Input current i_{in} and output voltage v_{C1} behavior under abrupt changes at the input voltage v_{in}	49
4.17	Instability in the source converter produced by the connection of a constant power load.	49
4.18	Source converter's input current i and output voltage v stabilization derived from modifying the control strategy.	50
4.19	Discrete-time algorithm for controller bank generation.	51
4.20	Stabilizing controller bank for $n = 40$	52
4.21	Multi-controller strategy implemented in PSIM.	53
4.22	Output behavior with (a) a single controller, (b) the multi-controller strategy. . .	53

Notation

I_q	Identity matrix of dimension $q \times q$.
A^\top	Transpose of matrix A .
$\text{col}(A, B)$	If A and B are matrices with the same number of columns, it denotes the matrix obtained by stacking A over B .
\mathbb{R}	Set of real numbers.
\mathbb{Z}	Set of integers.
\mathbb{Z}_+	Set of positive integers.
\mathbb{R}^q	Space of real vectors of dimension q .
$\mathbb{R}^{p \times q}$	Space of $p \times q$ dimensional real matrices.
$\mathbb{R}^{\bullet \times \bullet}$	Space of real matrices with an unspecified number of rows and columns.
$\text{rank}(A)$	Rank of a given matrix $A \in \mathbb{R}^{\bullet \times \bullet}$.
$\text{colspan}(A)$	Column span of A , i.e. the set of all possible linear combinations of its column vectors.
$(\sigma f)(t)$	<i>Shift operator</i> applied to a function $f : \mathbb{Z}_+ \rightarrow \mathbb{R}^q$. Defined as $(\sigma f)(t) := f(t + 1)$, and can be of order N in general, i.e. $(\sigma^N f)(t) := f(t + N)$.

Chapter 1

Introduction

In recent years, renewable energy research has been deemed as one of the key points to leading the planet into a more sustainable framework. The main motivation behind the growing use of renewables is to reduce dependence on fossil fuels and greenhouse gas emissions.

Power converters have thus been a core element of such research, since their usefulness lies in their ability to overcome some of the inherent limitations imposed by the use of renewable energy sources (e.g. low voltage outputs, intermittency caused by environmental conditions, difficulty of interconnection with other sources). As such, multiple strategies for *robust control* of power converters have been successfully implemented (see e.g. [2–4]).

However, a great number of these control schemes are tested on converters designed for stand-alone operation, i.e. considering a nominal resistive load connected at the output. Therefore, when these converters are connected to an integrated system, e.g. an energy distribution network, the interaction between subsystems may cause significant performance degradation, or – in the worst-case scenario – instability due to the *negative impedance* inherent to regulated power devices such as *constant power loads* (CPLs).

In order to mitigate such issues, we usually employ *model-based* paradigms; we assume that a model representing the full DC network is readily available for us to design stabilizing control strategies. Examples of such model-based approaches include: [2–4], where control structures are implemented in order to regulate boost converters feeding CPLs; [5–9], where the asymptotic stability of cascaded DC-DC converters is studied; [10–13], where efforts are made to mitigate the effect caused by negative impedance in a load converter, therefore inducing stability; [14–16], where new stabilization methods, such as damping enhancement and sliding mode control for CPL-loaded controllers, are introduced.

Evidently, these contributions center their theoretical development on the availability of a full network model, particularly in state space form, i.e. using sets of first order differential equations. It is well-known that there exists a high amount of available mathematical tools and environments compatible with state space representations. Moreover, the study of stability properties for such systems can be easily carried out by means of *linear matrix inequalities* (LMIs).

Following these ideas, the fact that such is the mainly used modeling approach is a natural consequence. Higher-order representations, on the other hand, are traditionally dropped in favor of first-order systems due to a shortage of mathematical and computational tools available for studying their dynamics and stability. [17]

However, *state space models of networks are not a given* [17], and in some cases their derivation is in a higher level of complexity, especially when introducing a higher number of state variables to the model or when considering the practical scenario of parasitic elements with energy storage or time delay properties; their presence in a circuit causes the addition of at least one more state variable or differential equation to the model. This challenge is recognized by researchers in the field of *smart grids* [18], who argue that traditional modeling techniques may not be entirely useful in studying scenarios where the complexity of networks becomes increasingly higher.

Prompted by these challenges, new *model-less* control techniques have surfaced in order to overcome the aforementioned modeling shortcomings. These techniques involve *data-driven* approaches that guarantee stability in a deterministic way, without the need for mathematical models. For example, [19] proposes data-driven control structures for interconnected microgrids by using measurement data and state observers. In [20], a generic model recreation for a microgrid is proposed by considering input/output measurement data.

The aforementioned solutions succeed in providing novel model-less approaches to stability; however, in most cases the technique requires either an identification of pre-defined mathematical models, or a high number of sensors due to the increasing number of state variables. Therefore, they do not consider the possibility of representing the full network dynamics and –a common occurrence in practice– with a limited number of sensors.

Motivated by these issues, in this thesis we present a data-driven deterministic approach to stability of power converters.

1.1 Overview of problem and contributions

It is known that a power converter tested in standalone design can be robustly regulated at a desired equilibrium point. However, as previously discussed, when the converter operates over a network, interconnections between subsystems cause a capacitor current

imbalance which destabilizes the previously stable capacitor voltage, thus steering the output into an undesirable behavior.

In order to mitigate this issue, our main contribution is to propose a framework where we adopt a general view of a network as a group of interconnected subsystems interacting with each other via electrical and control variables (currents, voltages and duty cycles respectively). Therefore, in order to design stabilizing controllers, we *zoom* into the network and focus on the to-be-controlled converter. This process is shown in Fig. 1.1.

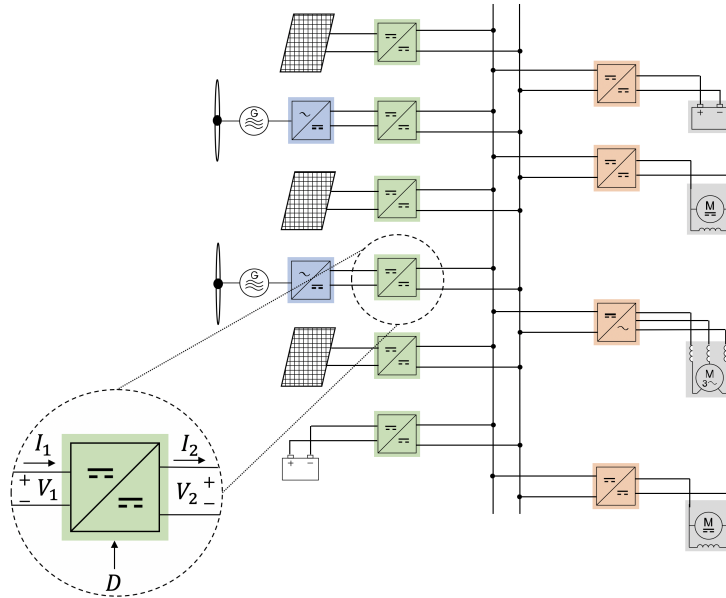


FIGURE 1.1: *Zooming* on DC-DC converter operating over a network for control purposes.

After zooming into a specific converter, we determine the variables of interest through which the subsystem interacts with the network. We then apply a *system identification* algorithm based on measured data from such converter variables, and use discrete-time Lyapunov theory in order to determine stabilizing controllers via solutions of a discrete-time LMI. Such a procedure allows for a mathematically rigorous re-designing of controllers whenever their behavior becomes unstable by network interconnections, i.e. in the CPL problem shown in [6, 21–24]. This strategy is depicted in Fig. 1.2.

As a secondary contribution, we benefit from the fact that solving the Lyapunov LMI in multiple instances during control design allows for the existence of multiple controller gain sets. These gain sets can be stored in a *controller bank* and used in the development of a *switching controller* framework.

As discussed in [1], the use switching control systems is motivated by a problem arising when, given a process typically described by a continuous-time control system, we need to find a controller such that the closed-loop system displays a desired behavior. In some cases, this feedback controller may not exist. In such situations, a possible alternative is to incorporate logic-based decisions into the control law and implement switching among

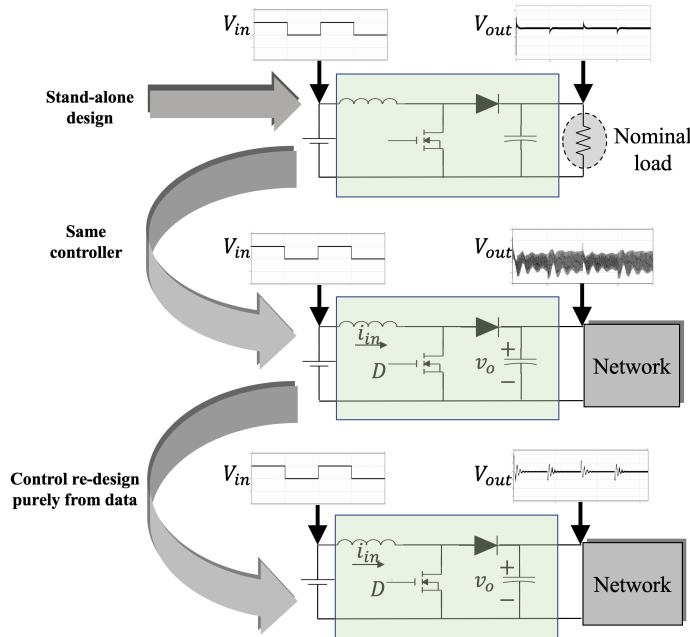


FIGURE 1.2: Controller re-design process via data-driven approach.

a *family of controllers*. Thus, a *hybrid* closed-loop system is generated, which is able to induce different sets of continuous-time dynamics based on discrete switching actions. Consider, for example, the case of *nonholonomic systems* described in [1]; such systems are subject to constraints involving both the state and its derivative. Therefore, they cannot be asymptotically stabilized by a continuous feedback controller.

We can single out the following motivating points in control problems for which we would need to consider switching control:

- In many realistic scenarios, continuous control is not suitable; i.e., there exist a set of desired dynamics which are not achievable by means of continuous control.
- The system model is highly uncertain, and a single continuous control law cannot be found.
- If a given process is prone to unpredictable external influences or component failures, then it may be necessary to consider discontinuous control as a way to ensure *adaptability* and *robustness* in the control scheme.

Based on these ideas, in this thesis we also present a switching, *adaptable* multi-controller strategy and test it on boost converters. Particularly, the family of controllers is generated by solving the Lyapunov stability problem in multiple instances, and the logic by which the controller switches into each possible scenario is given by an arbitrarily imposed *switching condition*, i.e. a logical decision-making step; this ensures adaptability in the control process. This is depicted schematically in Fig. 1.3.

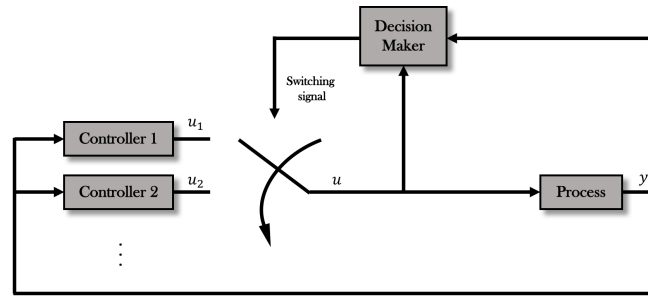


FIGURE 1.3: General diagram of switching control [1].

1.2 Objective of the thesis

Following the aforementioned ideas, the specific research objectives to which we contribute with this thesis are listed below:

- To develop a data-driven control strategy for DC-DC power converters (both in standalone and interconnected operations) which bypasses the need for mathematical models and guarantees asymptotic stability.
- To introduce a switching multi-controller framework which steers the plant output dynamics as close as possible to an unknown, desired trajectory.

1.3 Outline of the thesis

We now describe the contents of this thesis.

- *Chapter 2.* We review fundamental concepts related to average modeling, linearization and control of DC-DC power converters. We also introduce the notion of Lyapunov stability conditions as a mathematical tool for stabilizing gain computation. Finally, we propose new results regarding a switching multi-controller structure. In this chapter, theoretical material is verified with MATLAB simulations.
- *Chapter 3.* We begin the study of discrete time systems, introducing higher-order representations in *linear difference systems (LDS)*. Moreover, we establish *quadratic difference forms (QdFs)* as a means of studying stability properties of a LDS. Moreover, further analysis regarding Lyapunov stability theory is given and a discrete-time version of the conditions in Chapter 2 is developed.
- *Chapter 4.* We propose an approach to data-driven control of DC-DC converters. We introduce the notion of *data-based* matrices, and establish necessary conditions for a set of measured data to be *sufficiently informative* about the system dynamics

in order to recreate its model. With this recreated model, we develop an algorithm to stabilize converters both in standalone operation and when connected over networks. We also present results regarding a proposed switching multi-controller structure which uses data-driven controllers. In this chapter, theoretical material is verified by means of PSIM simulations and experimental validation.

- *Chapter 5.* We provide general conclusions and establish future research directions for the hereby presented work.

Appendix [A](#) contains all the MATLAB codes written for testing the theoretical material hereby developed.

Chapter 2

Continuous-time control of DC-DC converters

In this chapter we introduce general concepts of continuous-time power converter modeling and control. We focus our study on the boost converter and develop a control strategy using Lyapunov criteria; such an analysis is instrumental for building a framework around the key content of this thesis. Finally, we present a switching multi-controller algorithm which uses the same Lyapunov-based approach to guarantee plant stability under specific performance conditions.

2.1 Preliminary background material

For ease of reference and in order to make this work self-contained, we first introduce some fundamental theoretical material which will be continuously referred to for the remainder of this chapter.

2.1.1 State space representations

As discussed in [25], a state space representation for any linear, time-invariant system has the general form

$$\begin{aligned}\frac{d}{dt}x &= Ax + Bu ; \\ y &= Cx + Du ;\end{aligned}\tag{2.1}$$

where $x : \mathbb{R} \rightarrow \mathbb{R}^n$ is the *state vector* comprised of n state variables, $u : \mathbb{R} \rightarrow \mathbb{R}^m$ is the *input vector* comprised of m input variables, while $A \in \mathbb{R}^{n \times n}$, $B \in \mathbb{R}^{n \times m}$, $C \in \mathbb{R}^{p \times n}$ and $D \in \mathbb{R}^{p \times m}$ are *coefficient matrices*. Finally, $y : \mathbb{R} \rightarrow \mathbb{R}^p$ is referred to as the *output vector*.

Now consider the case where the input u is *state-dependent*, e.g. $u = -kx$ with $k \in \mathbb{R}^n$. By letting $C = 0$ and $D = 0$, then substituting u in (2.1), we obtain:

$$\frac{d}{dt}x = \hat{A}x ; \quad (2.2)$$

where $\hat{A} = (A - Bk) \in \mathbb{R}^{n \times n}$ is a new coefficient matrix. Due to the lack of an input in its model, (2.2) is commonly referred to as an *autonomous system*. In the following, we show how in state-space modeling, studying system stability requires a system to be autonomous.

2.1.2 Lyapunov stability theory

When controlling a given dynamical system, we are interested in studying its behavior in terms of stability. Thus, we first introduce a classic definition [26], i.e. a linear system represented by (2.2) is *asymptotically stable* if $\lim_{t \rightarrow \infty} x(t) = 0$ for all x that satisfies (2.2).

This definition allows for a general understanding of the implications behind stable system behavior. However, for control design purposes, it becomes necessary to study such a concept in terms of mathematical specifications. Therefore, we now introduce the notion of Lyapunov criteria:

Theorem 2.1. [26] A system represented by (2.2) is asymptotically stable if there exists a state function $V(x)$ such that, for all x that satisfies (2.2), it holds that: 1) $V(x) \geq 0$, and 2) $\frac{d}{dt}V(x) < 0$. Thus, $V(x)$ is called a *Lyapunov function* for (2.2).

Consider the autonomous system described by (2.2), and let the *candidate function* for Theorem 2.1 be the quadratic state function $V(x) = x^T P x$, where $P = P^T > 0$ is an unknown matrix. Taking the time derivative of the state function by means of the chain rule yields:

$$\begin{aligned} \frac{d}{dt}V(x) &= \frac{d}{dt}x^T P x + x^T P \frac{d}{dt}x \\ &= x^T \hat{A}^T P x + x^T P \hat{A} x \\ &= x^T (\hat{A}^T P + P \hat{A}) x . \end{aligned} \quad (2.3)$$

Thus, in order for Theorem 2.1 to hold, it must follow that

$$\hat{A}^T P + P \hat{A} < 0 . \quad (2.4)$$

Notice that (2.4) is known as a *linear matrix inequality* (LMI). Therefore, given any linear system, its stability can be verified by numerically computing a matrix P which satisfies (2.4). This can be done by means of standard LMI solvers, such as Yalmip [27]. Such a toolbox consists of an add-on to the numerical environment MATLAB, and

is used to solve feasibility problems related to linear inequalities with a specified set of constraints.

We have given a brief introduction to state-space representations and stability for dynamical models; in the following, we show how to obtain such models from DC-DC power converters.

2.2 Modeling of DC-DC power converters

We now discuss a procedure for determining mathematical models describing power converter dynamics in a rigorous manner. We first focus on *large-signal* modeling in order to describe such converters in terms of the underlying nonlinear equations. Then we study *small-signal* modeling, which approximates the large-signal behavior with linear equations. Note that the latter is particularly useful when attempting control design on power converters.

2.2.1 Large-signal modeling

Let us consider the traditional boost converter with a nominal resistive load, as depicted in Fig. 2.1.

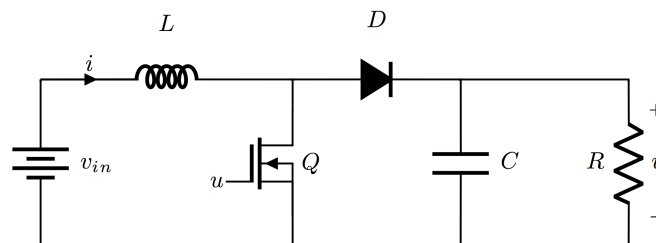


FIGURE 2.1: Traditional boost converter topology.

The values of the discrete switching variable $u \in \{0, 1\}$ induces two possible circuit topologies, as illustrated in Fig. 2.2. Thus, we can obtain their dynamics by applying Kirchhoff's laws in each case.

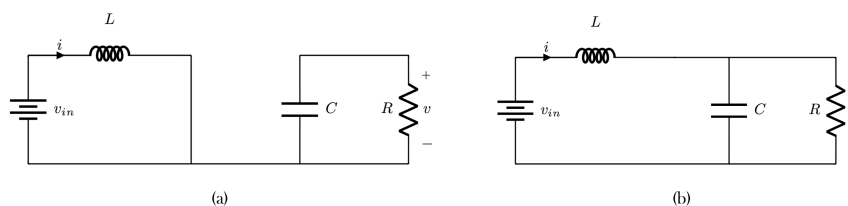


FIGURE 2.2: Topologies induced by switching.

Consider the circuit in Fig. 2.2 a. When the switching variable is set to $u = 1$, Kirchhoff's voltage and current laws yield the following dynamics:

$$\begin{cases} L \frac{d}{dt} i = v_{in} \\ C \frac{d}{dt} v = -\frac{v}{R} \end{cases} \quad (2.5)$$

Conversely, let us now consider the circuit in Fig. 2.2 b. When the switching variable is set to $u = 0$, Kirchoff's voltage and current laws yield the following dynamics:

$$\begin{cases} L \frac{d}{dt} i = -v + v_{in} , \\ C \frac{d}{dt} v = i - \frac{v}{R} . \end{cases} \quad (2.6)$$

By comparing both sets of equations and introducing the switching variable u as a parameter, we obtain a unified dynamic model for the circuit, described by:

$$\begin{cases} L \frac{d}{dt} i = -(1-u)v + v_{in} , \\ C \frac{d}{dt} v = (1-u)i - \frac{v}{R} . \end{cases} \quad (2.7)$$

Equation set (2.7) represents the *switched model* of the boost converter. This representation emphasizes the discrete nature of the input variable u . However, when working with periodic switching signals, it becomes necessary to consider the *average value* of the input variable over a switching time period [28]. Therefore, the previously discrete switching variable u now becomes a continuous average switching variable, i.e. $d \in [0, 1]$. We refer to d as the *duty cycle*.

Finally, we obtain the *average model* of the boost converter by replacing the discrete switching variable in the switched model (2.7) with its continuous equivalent: the duty cycle. Thus, the average model is given by

$$\begin{cases} \frac{d}{dt} i = \frac{-(1-d)}{L} v + \frac{v_{in}}{L} , \\ \frac{d}{dt} v = \frac{(1-d)}{C} i - \frac{1}{RC} v . \end{cases} \quad (2.8)$$

Notice that multiplication between variables makes such a model nonlinear.

Remark 2.2. In equation sets (2.5 - 2.7), state variables $[i \ v]$ are defined as *instantaneous*. However, when used in (2.8) –and for the rest of this thesis–, such variables are reformulated in *average* terms.

2.2.2 Small-signal modeling: Approximate linearization

Through a *linearization* process, nonlinear models can be approximated –around a specific point– by a linear equivalent. However, this new model is only valid in a region near

the selected point. As discussed in [28], in nonlinear DC-DC power converters, approximate linearization-based feedback controllers usually perform stabilization to a desired equilibrium value even when the dynamics of the controlled converter start at the origin, i.e. when the initial conditions of such a system are far away from such an equilibrium. This optimal performance can be attributed to the fact that DC-DC power converters have one single equilibrium point for each input/output variable, unlike highly nonlinear systems which could possibly have a larger number of equilibria (e.g. Furuta pendulum). Based on these ideas, we derive a linearized model in order to design a controller for a nonlinear boost converter.

Let $u : \mathbb{R} \rightarrow \mathbb{R}^m$ and $y : \mathbb{R} \rightarrow \mathbb{R}^n$ be the input/output variables available in a system. In a boost converter, the input $u := d$ is the duty cycle, and the output $y := \text{col}(i, v)$ contains the input current and output voltage. Thus, let $w := \text{col}(u, y)$ be the global set of variables of interest in a boost converter.

Consider the boost converter model described by (2.8). We can begin to linearize this model about an arbitrary equilibrium point by defining *error variables* for each input/output in the nonlinear system, i.e.

$$\hat{w} := w - \bar{w} ;$$

where \bar{w} contains the values of the variable set at the fixed equilibrium. The following analogous notation for the input-output partition is used:

$$\hat{w} = \text{col}(\hat{u}, \hat{y}) .$$

Finally, we can complete the linearization process by performing a Taylor series expansion of (2.8). For ease of reference, we recall the theoretical details behind such a concept.

Consider a dynamical system described in general by

$$\frac{d}{dt}y_k = f_k(y_1, y_2, \dots, y_n, u_1, u_2, \dots, u_m), k = 1, 2, \dots, n ,$$

with error variables \hat{y} and \hat{u} . A *Taylor series expansion* of f_k about the equilibrium points such that $f_k(\bar{y}_1, \bar{y}_2, \dots, \bar{y}_n, \bar{u}_1, \bar{u}_2, \dots, \bar{u}_m) = 0$, is given by

$$\frac{d}{dt}\hat{y}_k = \left(\sum_{j=1}^n \frac{\partial f_k}{\partial y_j} \hat{y}_j + \sum_{j=1}^m \frac{\partial f_k}{\partial u_j} \hat{u}_j \right) \Bigg|_{\substack{y=\bar{y} \\ u=\bar{u}}} \quad (2.9)$$

Now consider the nonlinear boost converter model in (2.8). As per (2.9), we can linearize this model about equilibria $\bar{i}, \bar{v}, \bar{d}$. Taking partial derivatives and evaluating at the corresponding equilibria yields the *linearized model* of the boost converter, given by:

$$\begin{cases} \frac{d}{dt}\hat{i} = -\frac{(1-\bar{d})}{L}\hat{v} + \frac{\bar{v}}{L}\hat{d}, \\ \frac{d}{dt}\hat{v} = \frac{(1-\bar{d})}{C}\hat{i} - \frac{1}{RC}\hat{v} - \frac{\bar{i}}{C}\hat{d}. \end{cases} \quad (2.10)$$

2.3 Control of DC-DC power converters

We now use the aforementioned linearized converter model in order to generate linear feedback controllers which, when interconnected with a nonlinear converter model, guarantee asymptotic stability by means of Lyapunov criteria.

2.3.1 Linear control design

In this analysis we do not impose a particular controller structure (*proportional (P)*, *proportional-integral (PI)*, *proportional-integral-derivative (PID)*), but instead we adopt a general point of view for control design and let the specific application dictate the type of controller to be used. Therefore, a feedback controller can adopt a general form

$$\begin{cases} \frac{d}{dt}z = Ez + Fu', \\ y' = Gz + Hu'; \end{cases} \quad (2.11)$$

where $z : \mathbb{R} \rightarrow \mathbb{R}^p$, $E \in \mathbb{R}^{p \times p}$, $F \in \mathbb{R}^{p \times n}$, $G \in \mathbb{R}^{m \times p}$, $H \in \mathbb{R}^{m \times n}$. In order to perform an interconnection between such a controller and a linear plant e.g. (2.1), let us define the controller input/output variables as $u' := y$ and $y' := u$, respectively. This process is depicted in Fig. 2.3.

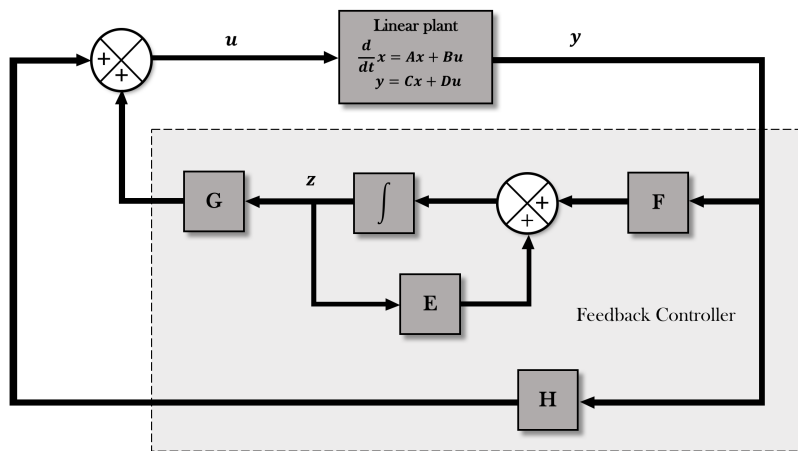


FIGURE 2.3: General feedback controller for a linearized converter.

Note that this general family of controllers admits any *P*, *PI*, *PID*, state- and output-feedback configurations, among many other suitable possibilities.

Let us now consider the linear plant in (2.1), as well as the controller in (2.11). By redefining the controller variables as shown in Fig. 2.3, we obtain the complete set of equations describing the plant-controller combination:

$$\begin{cases} \frac{d}{dt}x = Ax + Bu ; \\ \frac{d}{dt}z = Ez + Fx ; \\ u = Gz + Hx . \end{cases} \quad (2.12)$$

By straightforward algebraic manipulation of (2.12), the general plant-controller combination can thus be represented as:

$$\frac{d}{dt} \begin{bmatrix} x \\ z \end{bmatrix} = \begin{bmatrix} A + BH & BG \\ E & F \end{bmatrix} \begin{bmatrix} x \\ z \end{bmatrix} . \quad (2.13)$$

2.3.2 Commercial boost converter control: Gain tuning

The general plant-controller structure in (2.12) allows us to proceed without imposing a particular control scheme, but instead letting the specific application be the determining factor for such a decision. Let us consider the particular case of a commercial boost converter whose manufacturer's pre-defined controller only allows for gain modification and consists of a double loop current-voltage nested controller, as depicted in Fig. 2.4.

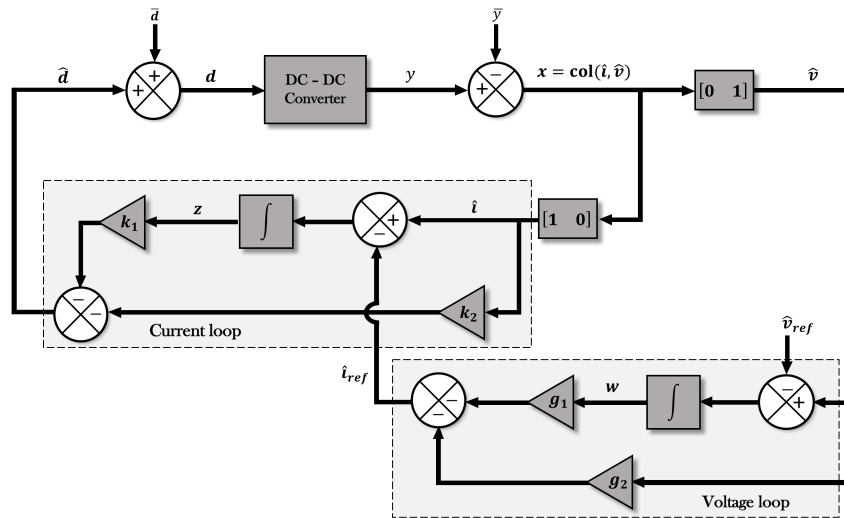


FIGURE 2.4: Predefined feedback controller example.

We observe that such a controller consists of the following equations:

$$\text{Voltage loop: } \begin{cases} \frac{d}{dt}w = \hat{v} - \hat{v}_{ref} , \\ \hat{i}_{ref} = -g_1 w - g_2 \hat{v} ; \end{cases} \quad (2.14)$$

$$\text{Current loop: } \begin{cases} \frac{d}{dt}z = \hat{i} - \hat{i}_{ref} , \\ \hat{d} = -k_1z - k_2\hat{i} ; \end{cases} \quad (2.15)$$

where $w, z : \mathbb{Z}_+ \rightarrow \mathbb{R}$ and $k_i, g_i, i = 1, 2$, are scalar quantities known as *gains*. Given this set of equations and considering the general state space model for linearized converters

$$\frac{d}{dt}x = Ax + Bu ,$$

by recalling that $x := \text{col}(\hat{i}, \hat{v})$ and letting $u := \hat{d}$, we can construct the converter-controller combined model:

$$\underbrace{\frac{d}{dt} \begin{bmatrix} x \\ z \\ w \end{bmatrix}}_{\frac{d}{dt}x'} = \underbrace{\begin{bmatrix} A - k_2B[1 \ 0] & -k_1 & 0_{2 \times 1} \\ [1 \ 0] + g_2[0 \ 1] & 0 & g_1 \\ [0 \ 1] & 0 & 0 \end{bmatrix}}_{\hat{A}} \underbrace{\begin{bmatrix} x \\ z \\ w \end{bmatrix}}_{x'} . \quad (2.16)$$

Controller gains $k_i, g_i, i = 1, 2$, which guarantee converter stability, can thus be computed using (2.4). Since in this case parameters from both \hat{A} and P are unknown, condition (2.4) is a *bilinear matrix inequality* whose solutions can be computed using standard LMI solvers such as `Yalmip`.

2.4 Multi-controller system

As discussed in Chapter 1, a special category of hybrid systems known as *switched systems*, considers continuous-time systems coupled with discrete switching events. Thus, we will now focus on the development of a switched multi-controller operation for a controlled converter such as the one described by (2.16).

In order to further understand the proposed multi-controller framework, we briefly recall the motivation behind its development. In Chapter 1, we argue that discontinuous control schemes allow for achievements in dynamics which are not possible using purely continuous feedback. Moreover, due to the logic-based part of its operation, switching control brings a sense of adaptability to the overall scenario. In terms of power converters, discontinuous feedback allows for a more robust variable (e.g. voltage) regulation despite abrupt changes in the load, in comparison to continuous control methods which may not respond as adequately.

Moreover, a multi-controller framework is also useful in cases where we become interested in *trajectory tracking* for any purpose; notable examples of such a situation are techniques such as *maximum power point tracking* [29] and *enveloped tracking*[30]. Constant voltage regulation –a common objective in power converter control– is not the main purpose in

these cases; they instead focus on following specific trajectory. For such purpose, an adaptable discontinuous controller is a plausible solution.

Following the above ideas, the concept of switching control can be applied to a controlled boost converter as in (2.16) by noticing that the stability condition in (2.4) is an *inequality*, i.e. it allows for multiple solutions. Therefore, by solving such an inequality and thus performing gain computation in multiple instances, we generate a “bank” or “family” of admissible (i.e. stabilizing) controller gains which will guarantee asymptotic stability when applied to the boost converter.

Having multiple gain sets implies the existence of various possible control scenarios (one for each gain set); these scenarios can be *switched into* depending on a state-related condition. Evidently, each of these control scenarios will steer the plant into a new set of asymptotically stable dynamics. We now introduce the preliminaries for the switching condition.

Let the *instantaneous error* $E(t)$ be defined as:

$$E(t) = | y(t) - y^*(t) | , \quad (2.17)$$

where:

- $y(t)$ is the instantaneous converter output (e.g. output voltage);
- $y^*(t)$ is a *desired trajectory*.

We therefore establish the *switching condition* for the multi-controller system as:

$$| E(5nT) - E(5(n-1)T) | \leq \epsilon , \quad (2.18)$$

where:

- $n = 1, 2, \dots$ is a scalar quantity measuring time steps;
- T denotes the integration step for the numerical method used to solve the dynamical model;
- ϵ is a scalar quantity known as *performance condition* for the multi-controller system, and is associated to the maximum allowed error rate between the real and desired dynamics.

As depicted in Fig. 2.5, condition (2.18) is used to induce switching between different controller gain sets based on the difference between the *real output* and an arbitrary *desired trajectory*. This *instantaneous error* is compared every 5 time steps and is

equivalent to measuring the *derivative* of the error variable. If such a derivative exceeds an admissible value ϵ , the system will switch into a different set of controller gains in an attempt to reduce future propagation of the error. In other words, the goal of this switched system is to steer the output “as close as possible” to an arbitrary desired behavior, by switching between controller gain sets when the rate of change of the error becomes unacceptable for the expected performance conditions.

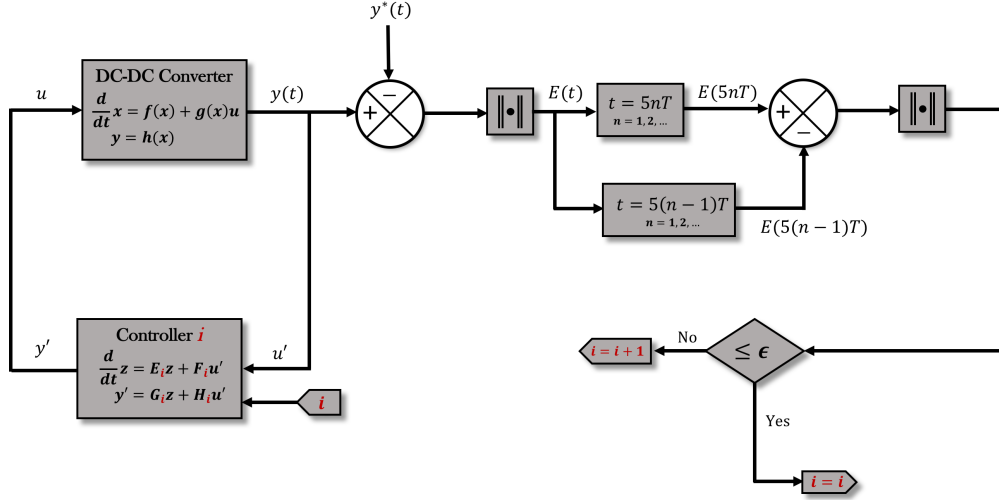


FIGURE 2.5: Multi-controller operation.

Remark 2.3. In this work we ponder the following classic considerations for switching multi-controller systems:

- To ensure stability, multiple plant-controller combined systems could share a common Lyapunov function.
- To ensure stability, multiple plant-controller combined systems could have a multiple Lyapunov function.
- Between switching instants, a certain dwell time must be considered in order for the system to approximate the equilibrium as much as possible; this prevents instability. In this work, we consider the dwell time to be $5nT$.

However, since these points are not part of the main scope of this thesis, we refer the reader to [31] for more details.

2.5 Simulation Results

Simulations were carried out in order to verify the theoretical material discussed above. In the case of continuous-time systems, we use the standard numerical environment MATLAB to test the validity of every concept described in this chapter.

2.5.1 Open loop traditional boost converter

As previously discussed and given the focus of this chapter, we first simulate a traditional boost converter in open-loop configuration as depicted in Fig. 2.1, with the nominal parameters shown in Table 2.1.

TABLE 2.1: Nominal parameters for simulation.

Notation	Parameter description	Value
V_{in}	Input voltage	30V
\bar{V}	Output voltage at equilibrium	200V
L	Inductor	250 μ H
C	Capacitor	10 μ F
R	Load resistance	100 Ω
h	Time step for numerical method	1 μ s

We carry out this simulation using the average model described by equation set (2.8). Using such equations, we can easily verify that the *equilibrium* values for duty cycle and current must equal

$$\bar{d} = \frac{\bar{v} - v_{in}}{\bar{v}} = 0.85 ; \quad \bar{i} = \frac{\bar{v}}{R} \left(\frac{1}{1 - \bar{d}} \right) = 13.333 \text{ A} . \quad (2.19)$$

We use the Forward-Euler numerical method to perform the simulation, solving the boost converter model described by (2.8). Simulation results are shown in Fig. 2.6.

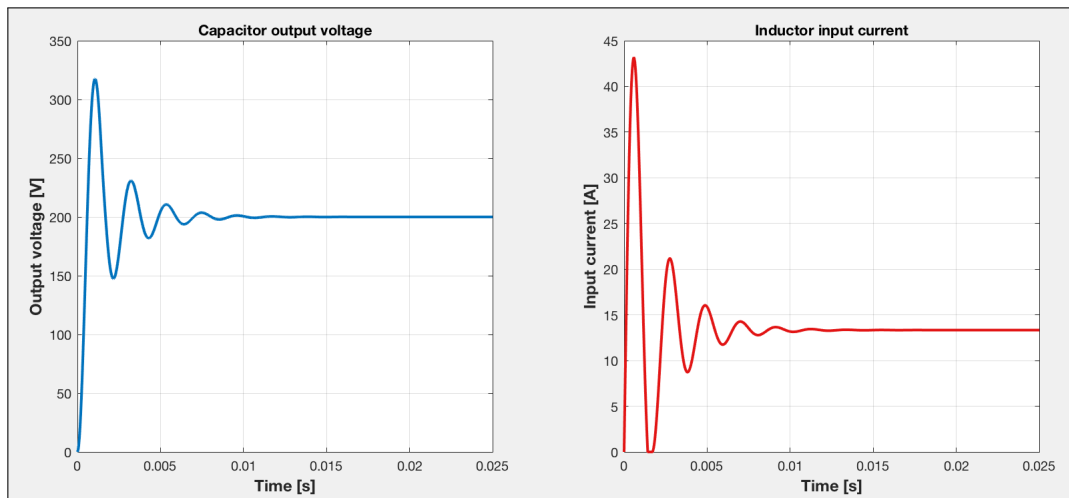


FIGURE 2.6: Boost converter simulation results.

Notice that the equilibrium values of both the voltage and the current in the simulation are as expected.

For a detailed description of the MATLAB codes written for simulation purposes, please refer to Appendix A.

2.5.2 Linear control of boost converter

We carry out a second simulation, now centered on solving the combined converter-controller model described by equation (2.16). The motivation behind this simulation is to test the validity of the ideas discussed in section 2.2.2, in which we argue that linear feedback controllers perform adequately when applied to nonlinear plants with a single equilibrium point, e.g. power converters.

To this purpose, consider the same boost converter as in Subsection 2.5.1, with nominal parameters described in Table 2.1 and equilibrium values defined in (2.19). From its linearized version described by (2.10), let the state space representation matrices

$$A := \begin{bmatrix} 0 & -\frac{(1-\bar{d})}{L} \\ \frac{(1-\bar{d})}{C} & -\frac{1}{RC} \end{bmatrix}; \quad B := \begin{bmatrix} \frac{\bar{v}}{L} \\ -\frac{\bar{i}}{C} \end{bmatrix}.$$

Such matrices can thus be used in the combined model described by (2.16). Moreover, using such a model's coefficient matrix, we solve the Lyapunov inequality (2.4) in order to compute stabilizing controller gains. Such a process yields the gain set

$$k_1 := 0.0047; \quad k_2 := 0.0141; \quad g_1 := 16.8823; \quad g_2 := 10.9711.$$

By recalling that these gains come from a linear model, we now use them in order to control the *nonlinear* system described by (2.8). To this purpose, we let the input $d := \hat{d} + \bar{d}$ and once again solve the nonlinear converter model by means of the Forward-Euler numerical method. Evidently, the value of d will vary with each iteration in order to satisfy the conditions of the control structure in (2.15). The results of this simulation are shown in Fig. 2.7.

Notice that aside from maintaining the voltage and current at the desired equilibrium points, the established control structure causes a relevant improvement in signal quality (particularly noticeable in the output voltage waveform) where the transient's overshoot, oscillation and response time are significantly reduced.

2.5.3 Multi-controller switching system

In Subsection 2.5.2 we focused on controlling a boost converter using Lyapunov stability criteria. We now extend this idea to a proof of concept regarding the multi-controller system discussed in section 2.4, where the inequality (2.4) is solved in multiple instances

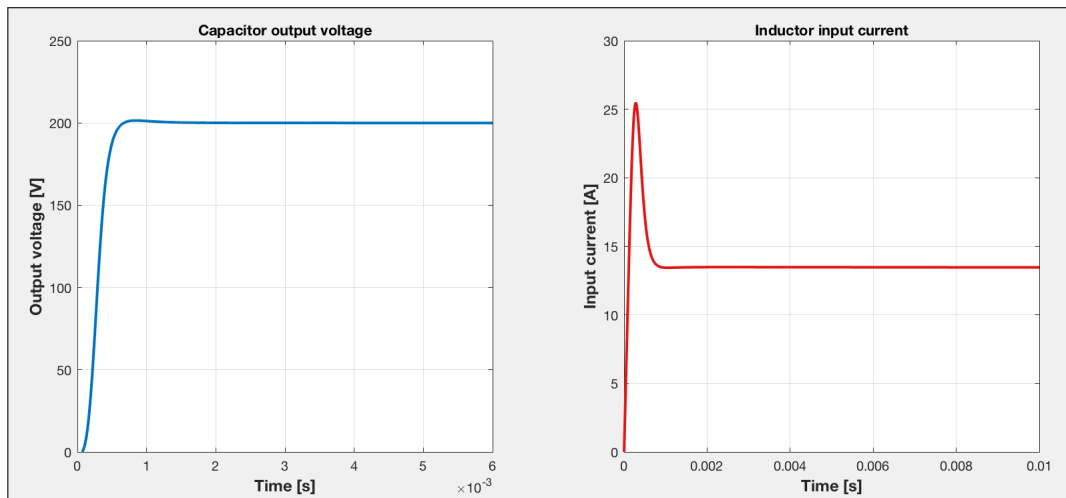


FIGURE 2.7: Controlled boost converter simulation results.

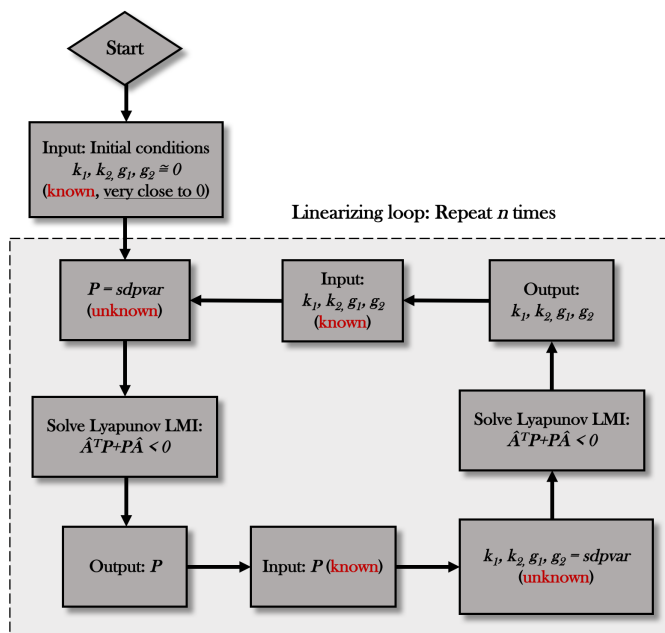


FIGURE 2.8: Algorithm for controller bank generation.

in order to generate a “bank” of admissible, stabilizing controllers for the converter. The general algorithm for this process is shown in Fig. 2.8.

The algorithm consists of a linearization of the bilinear matrix inequality (2.4); we achieve this by starting the algorithm with gain values (embedded in matrix \hat{A}) which are very close to 0, thus reducing the number of unknown parameters to one, i.e. matrix P , and effectively transforming the Lyapunov condition into a *linear matrix inequality* (LMI). After computing P , we use it as a known parameter to compute a new, unknown gain set. We then use such a gain set as a known parameter to compute a new P matrix. We refer to this process as a *linearizing loop*, which is repeated to generate n controller gain sets. Note that all n gain sets guarantee asymptotic stability, given that they are generated under Lyapunov criteria.

The process of computing multiple stabilizing gain sets leads to the generation of a *gain matrix* defined as

$$\mathfrak{C}_n := \begin{bmatrix} k_{1_1} & k_{2_1} & g_{1_1} & g_{2_1} \\ k_{1_2} & k_{2_2} & g_{1_2} & g_{2_2} \\ \vdots & \vdots & \vdots & \vdots \\ k_{1_n} & k_{2_n} & g_{1_n} & g_{2_n} \end{bmatrix};$$

whose n number of rows are comprised of the gain sets computed using the algorithm in Fig. 2.8.

Such an algorithm was used to compute multiple stabilizing gains for the same boost converter used in previous subsections (refer to Table 2.1 and (2.19) for parameters). Starting the algorithm with initial conditions

$$k_1 := 0.001; \quad k_2 := 0.0001; \quad g_1 := 0.0001; \quad g_2 := 0.0001,$$

we apply the algorithm in Fig. 2.8 by means of the Yalmip solver. For $n = 40$, Fig. 2.9 shows the gain matrix \mathfrak{C}_{40} in table form.

Row	k_1	k_2	g_1	g_2
1	0.00101	0.00027	0.01534	0.19807
2	0.00101	0.00017	0.08072	0.36001
3	0.00100	0.00012	0.14605	0.46742
4	0.00101	0.00015	0.30293	0.56033
5	0.00101	0.00015	0.49447	0.70160
6	0.00101	0.00011	0.71433	1.00751
7	0.00101	0.00014	0.90525	1.05200
8	0.00102	0.00017	1.07925	1.08330
9	0.00102	0.00015	1.09827	1.16012
10	0.00104	0.00019	1.28576	1.18603
11	0.00105	0.00023	1.45461	1.21443
12	0.00106	0.00020	1.41538	1.31896
13	0.00106	0.00017	1.41318	1.42988
14	0.00107	0.00015	1.43731	1.54569
15	0.00108	0.00018	1.61871	1.51012
16	0.00108	0.00016	1.62143	1.64112
17	0.00109	0.00020	1.79443	1.59516
18	0.00109	0.00017	1.78937	1.73217
19	0.00111	0.00021	1.95892	1.67696
20	0.00111	0.00019	1.94804	1.81623
21	0.00113	0.00023	2.11694	1.75333
22	0.00115	0.00028	2.26791	1.71057
23	0.00118	0.00035	2.43198	1.68739
24	0.00122	0.00043	2.60515	1.68484
25	0.00123	0.00039	2.52900	1.86047
26	0.00128	0.00048	2.72976	1.83665
27	0.00129	0.00045	2.68037	1.99670
28	0.00130	0.00043	2.66937	2.12947
29	0.00131	0.00041	2.67778	2.24258
30	0.00131	0.00040	2.69938	2.34079
31	0.00136	0.00049	2.96041	2.25742
32	0.00137	0.00048	2.97199	2.36857
33	0.00144	0.00058	3.24442	2.30566
34	0.00153	0.00069	3.53107	2.28135
35	0.00154	0.00067	3.51267	2.41725
36	0.00165	0.00078	3.83218	2.41161
37	0.00180	0.00091	4.21874	2.45165
38	0.00181	0.00089	4.19443	2.59186
39	0.00198	0.00102	4.63005	2.65503
40	0.00217	0.00114	5.11772	2.75734

FIGURE 2.9: Stabilizing controller bank for $n = 40$.

Notice that even though the algorithm starts at values which are practically zero, the values of $k_i, g_i, i = 1, 2$ exhibit linear convergence to an unknown value as we repeatedly solve the gain computation algorithm. Even though the final value of convergence is uncertain, we do not focus on unraveling it; rather, we take advantage of the fact that this convergence process provides us with various controller gains which guarantee asymptotic stability for the boost converter.

As discussed in section 2.4, having multiple controller gains implies the possibility of creating a control system which switches into each gain set according to a certain performance condition; we simulate such an idea as a proof of concept using the same boost converter as in previous subsections.

Consider the controlled boost converter in section 2.5.2. Using MATLAB, we extend such a simulation to include the multi-controller system; namely, we consider the gain matrix \mathbf{C}_{40} shown in Fig. 2.9 as well as condition (2.18) for automatic switching into each gain set. We establish the *desired trajectory* to be

$$y^*(t) = 200[1 - e^{-290t} \cos(700t)] ,$$

as well as a maximum allowed error rate of $\epsilon = 0.1$. Results of this simulation are shown in Fig. 2.10. Notice that, as expected by design, the multi-controller system steers the output as close to the desired trajectory as possible within the allowed error rate.

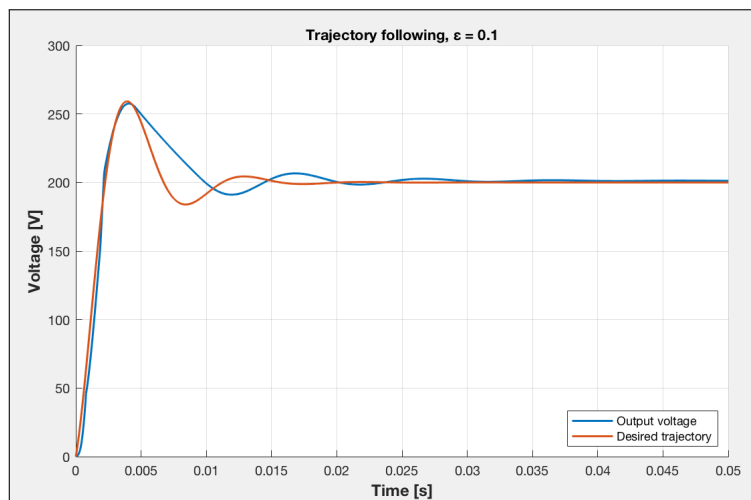


FIGURE 2.10: Multi-controller structure performance for $\epsilon = 0.1$.

As a further proof of concept and in order to show a fundamental effect of changing the desired trajectory's oscillating frequency, we repeat the previous simulation with different parameters. Consider the desired trajectory

$$y^*(t) = 200[1 - e^{-40t} \cos(700t)] ,$$

and a new performance condition $\epsilon = 0.01$. Results of this simulation are shown in Fig. 2.11. Notice that when dealing with waveforms that exhibit higher oscillation frequencies, it becomes increasingly difficult for the output to precisely follow the desired trajectory despite it being subjected to a stricter maximum allowed error rate.

We now consider the case of a multi-controller system with a varying performance condition. Let a desired trajectory

$$y^*(t) = 200[1 - e^{-40t} \cos(400t)] ,$$

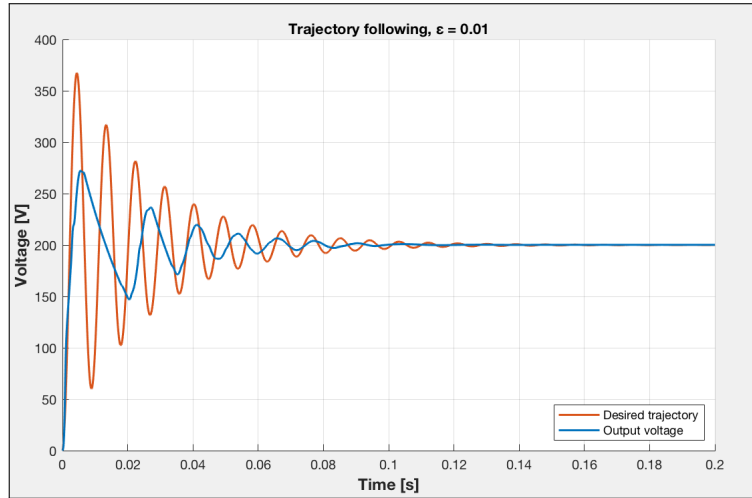


FIGURE 2.11: Multi-controller structure performance for $\epsilon = 0.01$ and different trajectory.

and a varying performance condition $\epsilon \in \{0.3, 0.2, 0.01\}$. We endeavor to compare the multi-controller system's performance when subjected to a decreasing (i.e. gradually stricter) maximum allowed error rate. The first condition, $\epsilon = 0.3$, yields the results shown in Fig. 2.12. Notice that, as expected, the multi-controller system switches between gain sets within the allowed error rate.

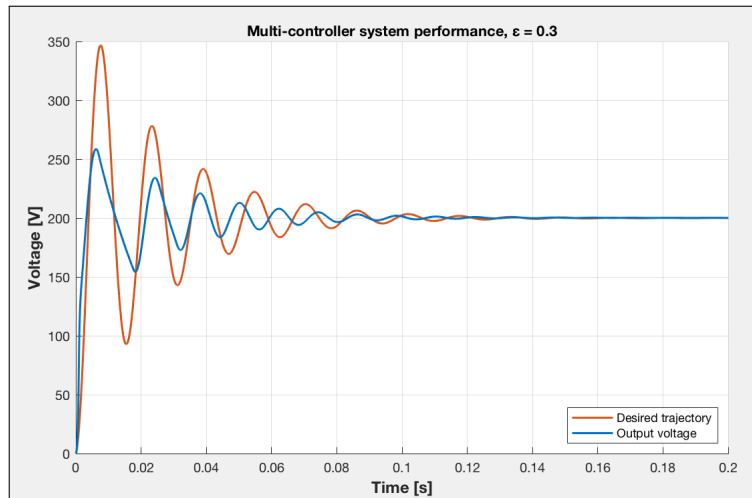
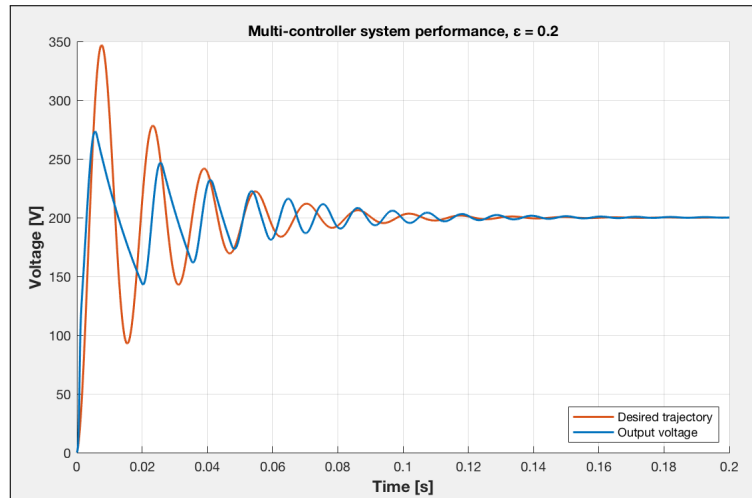
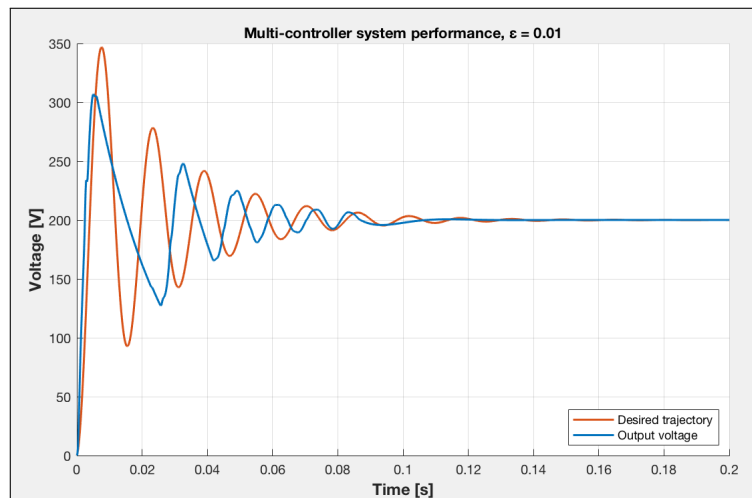


FIGURE 2.12: Multi-controller structure performance for varying ϵ (0.3).

We now reduce the allowed error, $\epsilon = 0.2$, showing the results in Fig. 2.13. Notice that decreasing ϵ evidently causes the system to switch controllers at a higher frequency, thus changing the plant dynamics to closely resemble the desired ones.

We finally analyze the case where the performance condition is reduced to $\epsilon = 0.01$, i.e. the strictest in this study. Fig. 2.14 shows that, once again, switching between controllers a higher number of times than the previous cases steers the plant dynamics as close as possible to the imposed trajectory.

FIGURE 2.13: Multi-controller structure performance for varying ϵ (0.2).FIGURE 2.14: Multi-controller structure performance for varying ϵ (0.01).

We now endeavor to test the multi-controller system's performance under disturbances. The first case is shown in Fig. 2.15, where we divide the output resistance by a factor of 10 starting at $t = 0.4s$. Moreover, the results show that the multi-controller system is able to regulate the output voltage despite abrupt changes in the load.

We now test disturbance rejection to changes in the input voltage, which was increased by 10 V at time instant $t = 0.6s$ and decreased by 20 V at time instant $t = 1s$. Fig. shows that the multi-controller system is also able to regulate abrupt changes at the input and maintain the output voltage at a constant value. Note that in both cases, the control scheme effectively switches between gain sets under the presence of external disturbances, thus showing robustness and adaptability.

We finally endeavor to test *trajectory following* for the multi-controller system, i.e., the case where the plant mimics an imposed behavior. For such a purpose, we define the to-be-tracked trajectory as

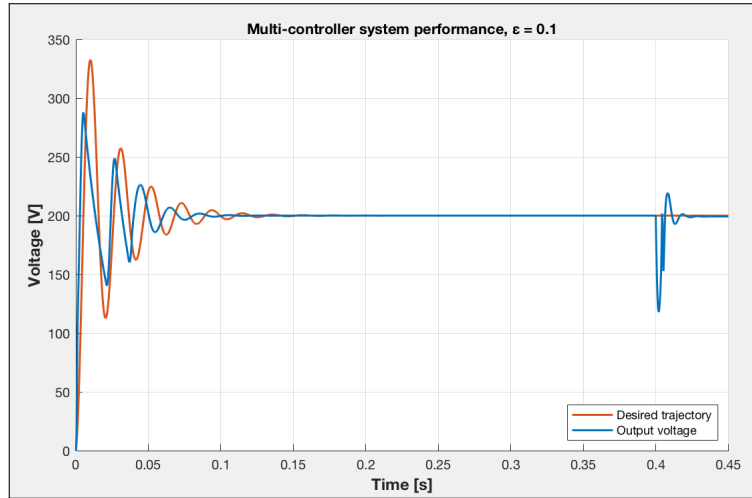


FIGURE 2.15: Multi-controller performance under abrupt changes in output resistance.

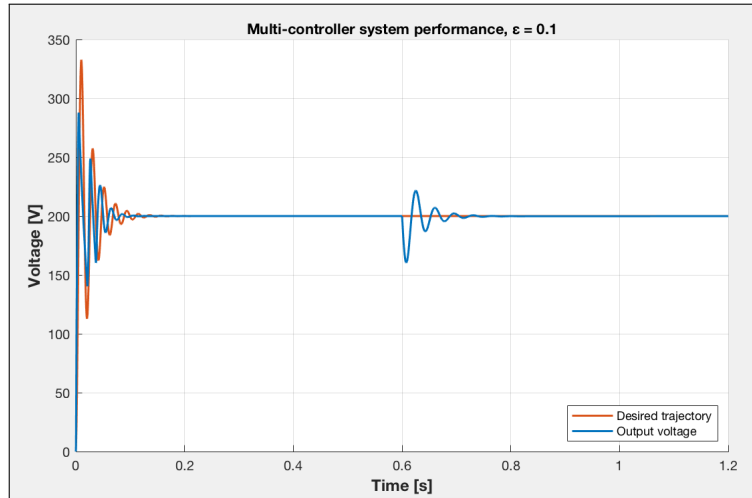


FIGURE 2.16: Multi-controller performance under abrupt changes in input voltage.

$$y^*(t) = 200[1 - e^{-20t} \cos(100t)].$$

In this case, during each iteration of the numerical method we change the equilibrium value to be that of $y^*(t_c)$, where t_c is the current time instant. Fig. 2.17 shows the results of such a simulation, where the varying equilibrium value induces trajectory following. For this particular simulation, a larger controller bank \mathfrak{C}_{500} was generated. Notice that the resistance-changing disturbance was also included in order to likewise test robustness and adaptability.

Fig. 2.18 depicts the multi-controller index i changing over time in accordance with the established switching condition. Note that the value remains constant in specific regions, while increasing linearly in others. There is a sudden change in value after $i = 500$; this is due to the re-initialization of the controller bank when reaching its maximum possible value.

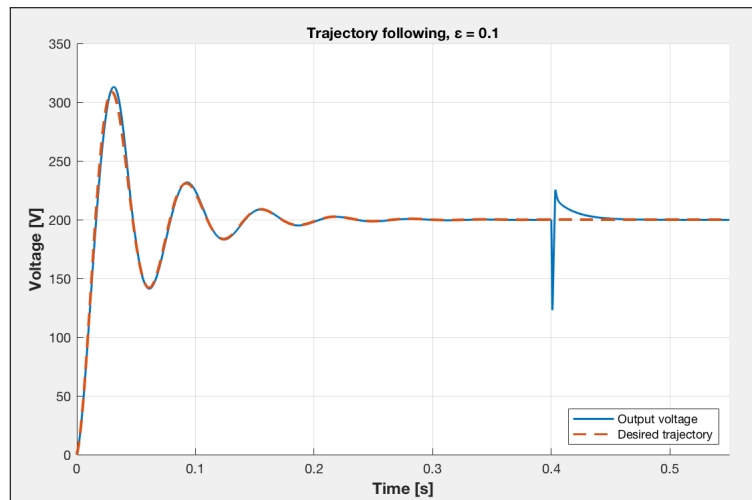
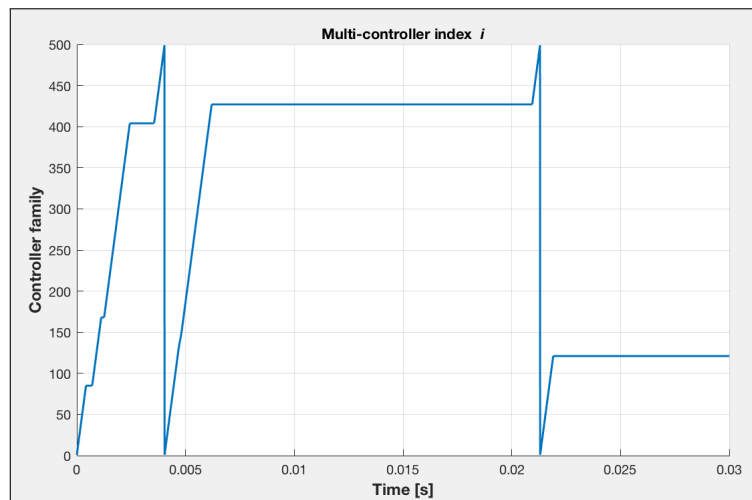


FIGURE 2.17: Multi-controller performance for trajectory following.

FIGURE 2.18: Changes in controller set index i for multi-controller system.

2.6 Conclusion

In this chapter, we examined preliminary concepts related to modeling and control of power converters. Namely, we discussed dynamical system theory, average modeling, linear control design and stability criteria. We showed that, for a general case, stability of a converter model can be determined by using control design via Lyapunov LMIs.

Moreover, we developed a switching multi-controller approach to power converter control in order to ensure adaptability and perform trajectory following when necessary. Note that in this chapter, even though we work in a continuous-time framework, switching conditions for the multi-controller system –namely (2.18)– are defined in terms of *discrete-time* variables. This approach is satisfactory in part since all models are solved by means of a numerical method, which is discrete by nature.

Despite the inconsistency brought by the combination of different time domains, we recognize that a modeling scenario as simple as a two-equation converter in state space is well-functioning. However, in more highly complex (model-wise) scenarios, a discrete-time framework appears to be the optimal way to formulate future work in order to maintain consistency.

Thus, in the following we examine the preliminaries of the main contribution in this thesis, where we use some of the previously discussed theory and apply it to *data-based*, model-less frameworks. To such purpose, we will study discrete-time, higher-order systems, i.e. the most natural way to work when processing data.

Chapter 3

Behavioral system theory

In the past chapter we introduced some concepts which are fundamental for the proper understanding of power converter control in general. We have focused solely on continuous time systems with state-space representations; however, the main results in this thesis are developed using a discrete-time framework and then applied in practice to continuous-time systems, e.g. power converters.

Therefore, in this chapter we will begin the study of discrete-time systems. We introduce general concepts of behavioral system theory which are fundamental for the development of our main contribution: data-driven controllers.

3.1 Linear difference systems

As previously established, a data-driven control approach requires the processing of measured/sampled data. Since we are dealing with sampled data over a time period, the most natural manner in which to model their dynamics is in terms of *discrete-time higher-order systems*. Moreover, we are dealing with cases in which a to-be-controlled model is not readily available (e.g. to represent in state space form); thus, in this study we drop state space techniques in favor of modeling based on linear difference systems.

Formally, a *linear difference system* can be expressed as

$$R_0 w + R_1(\sigma w) + \cdots + R_N(\sigma^N w) = 0, \quad (3.1)$$

where:

- $w : \mathbb{Z}_+ \rightarrow \mathbb{R}^q$ is the function mapping discrete time points to the q measured variables (e.g. voltages/currents), which can then be expressed as a finite time series $w(1), w(2), \dots, w(T)$ with sampling period T .

- σ is called the *shift operator*, analogous to the continuous-time derivative operator. It is defined as $(\sigma f)(t) := f(t+1)$, which can generally be of order N (also known as *lag*), i.e., $(\sigma^N f)(t) := f(t+N)$.
- $R_i \in \mathbb{R}^{p \times q}$, with $i = 0, 1, \dots, N$ are called *coefficient matrices*.

Equation (3.1) also admits a *kernel representation*; thus, it can be written in a compact way as

$$R(\sigma)w = 0, \quad (3.2)$$

where $R(\sigma)$ is a polynomial matrix of degree N and represents a dynamical relationship among the discrete-time set of measured data w .

Note that state space modeling is a special case of (3.2). For example, given a model

$$\sigma x = Ax + Bu,$$

if $w := \text{col}(x, u)$, then $R(\sigma) := \begin{bmatrix} \sigma I - A & -B \end{bmatrix}$.

As its name implies, behavioral system theory studies a dynamical system in terms of its *behavior*, i.e. the set of admissible trajectories which an input-output system can generate based on a set of laws that govern it.

Thus, in this case the *behavior of a system*, denoted by \mathfrak{B} , can be formally defined in terms of trajectories as

$$\mathfrak{B} := \{w : \mathbb{Z}_+ \rightarrow \mathbb{R}^q \mid R(\sigma)w = 0\}; \quad (3.3)$$

where w is a column vector of the measured variables.

3.2 Quadratic difference forms

Given a linear difference system as in (3.2), in some cases it becomes necessary to deal with *functionals* of w and its time-shifts. For example and particularly important to this section, Lyapunov functions for higher order difference equations often require the analysis of quadratic functionals for stability purposes. Given that in this chapter we focus our efforts on employing higher-order representations as opposed to state-space, we are inclined to consider quadratic state functionals.

We thus introduce the notion of *quadratic difference forms* [32], by means of which we can study the stability properties of linear difference systems.

A *quadratic difference form* (QdF) is a functional of the discrete-time variable w and its time-shifts:

$$Q_K(w) := \begin{bmatrix} w^\top & \sigma w^\top & \dots & \sigma^{N-1} w^\top \end{bmatrix} K \begin{bmatrix} w \\ \sigma w \\ \vdots \\ \sigma^{N-1} w \end{bmatrix}, \quad (3.4)$$

where $K = K^\top$ is known as a *coefficient matrix* with dimension $Nq \times Nq$.

Analogous to the continuous-time derivative, the discrete-time *rate of change* ∇Q_K of a QdF Q_K is defined as

$$\nabla Q_K(w)(t) := \sigma Q_K(w)(t) - Q_K(w)(t);$$

where the QdF σQ_K is called a time-shift of Q_K and has a coefficient matrix K' [32], which is defined as:

$$K' := \begin{bmatrix} 0_{q \times q} & 0_{q \times Nq} \\ 0_{Nq \times q} & K \end{bmatrix}. \quad (3.5)$$

We finally use such a coefficient matrix in order to define the QdF σQ_K as

$$\sigma Q_K(w) := \begin{bmatrix} w^\top & \sigma w^\top & \dots & \sigma^N w^\top \end{bmatrix} K' \begin{bmatrix} w \\ \sigma w \\ \vdots \\ \sigma^N w \end{bmatrix}. \quad (3.6)$$

3.3 Lyapunov stability criteria

As in the previous chapter, we use a common definition for system stability. A system represented by (3.2) is *asymptotically stable* if $\lim_{t \rightarrow \infty} w(t) = 0$ for all w that satisfies (3.2).

We now use Lyapunov conditions to develop mathematical specifications for stability. Given Theorem 2.1, we can adapt it to systems whose stability is studied by means of QdFs:

Theorem 3.1. [32] *A system represented by (3.2) is asymptotically stable if there exists a QdF Q_K such that, for all w that satisfies (3.2), it holds that: 1) $Q_K \geq 0$; and 2) $\nabla Q_K < 0$.*

If Theorem 3.1 holds, then Q_K is called *Lyapunov function* for 3.2.

Notice that, as shown in [32], condition 2) in Theorem 3.1 holds if and only if there exists a QdF $Q_K > 0$, as well as polynomial matrices $Y(\sigma)$ and $D(\sigma) = D(\sigma)^\top$ of suitable sizes such that

$$\sigma Q_K(w) - Q_K(w) + w^\top R(\sigma)^\top Y(\sigma)w + w^\top Y(\sigma)^\top R(\sigma)w = -w^\top D(\sigma)^\top D(\sigma)w . \quad (3.7)$$

Note that, for every w that satisfies (3.2), it follows that

$$\underbrace{\sigma Q_K(w) - Q_K(w)}_{\nabla Q_K} = -w^\top D(\sigma)^\top D(\sigma)w ;$$

which guarantees a negative rate of change due to the quadratic nature of the right-hand member of such an equation.

In a similar manner as we derive a stability condition for the continuous case (namely (2.4)) based on *inequalities*, we can extend this idea to the QdF-based stability condition in (3.7) by first noting that the left-hand member of (3.2) can be written as

$$R(\sigma)w = \begin{bmatrix} R_0 & R_1 & \cdots & R_N \end{bmatrix} \begin{bmatrix} w \\ \sigma w \\ \vdots \\ \sigma^N w \end{bmatrix} . \quad (3.8)$$

Therefore, we can define a *coefficient matrix* for (3.8) as

$$\tilde{R} := \begin{bmatrix} R_0 & R_1 & \cdots & R_N \end{bmatrix} . \quad (3.9)$$

Similarly, we can define a coefficient matrix for $Y(\sigma)$ in (3.7) as

$$\tilde{Y} := \begin{bmatrix} Y_0 & Y_1 & \cdots & Y_N \end{bmatrix} .$$

Moreover, we define

$$v^\top = \begin{bmatrix} w^\top & \sigma w^\top & \cdots & \sigma^N w^\top \end{bmatrix} .$$

Using these new coefficient matrices, as well as the definition of a QdF in (3.4) and its time-shift in (3.6), we can express the stability condition (3.7) as

$$\begin{aligned} & \overbrace{v^\top \begin{bmatrix} 0_{q \times q} & 0_{q \times Nq} \\ 0_{Nq \times q} & K \end{bmatrix} v}^{\sigma Q_K(w)} - \overbrace{v^\top \begin{bmatrix} K & 0_{Nq \times q} \\ 0_{q \times Nq} & 0_{q \times q} \end{bmatrix} v}^{Q_K(w)} \\ & + \underbrace{v^\top \tilde{R}^\top \tilde{Y} v + v^\top \tilde{Y}^\top \tilde{R} v}_{w^\top R(\sigma)^\top Y(\sigma)w + w^\top Y(\sigma)^\top R(\sigma)w} < 0 . \end{aligned}$$

Notice that the inequality “ < 0 ” is used in place of the right-hand member of (3.7) in order to maintain the required negative rate of change. By linear algebra principles, such a stability condition can be reduced to computing a matrix K which satisfies the following linear matrix inequality (LMI):

$$\begin{bmatrix} 0_{q \times q} & 0_{q \times Nq} \\ 0_{Nq \times q} & K \end{bmatrix} - \begin{bmatrix} K & 0_{Nq \times q} \\ 0_{q \times Nq} & 0_{q \times q} \end{bmatrix} + \tilde{R}^\top \tilde{Y} + \tilde{Y}^\top \tilde{R} < 0. \quad (3.10)$$

Notice that matrices K and \tilde{Y} can be numerically computed using standard LMI solvers such as Yalmip [27].

3.4 Conclusion

In this chapter, we introduced the basic concepts and notions regarding linear discrete time systems. This was done as a preamble of the main contribution in this thesis: data-driven control, which is naturally carried out using discrete time frameworks.

We also studied Lyapunov stability in terms of higher-order discrete systems. Note that the LMI in (3.10) is linear, and is therefore numerically simple to compute. On the other hand, from [31] we recall that, given a discrete autonomous system represented in state space e.g. $\sigma x = \hat{A}x$, its stability condition is described by

$$\hat{A}^\top P \hat{A} - P < 0;$$

which is quadratic by nature. Thus, from a numerical standpoint, its computation becomes highly difficult in comparison to the linear inequalities built from higher-order representations.

In this chapter we offered a solution to modeling and stability working purely from data, bypassing the need to implement state space techniques which are not always imperative or essential. In the following, we apply the material developed in this chapter in the context of dynamic system control purely from data.

Chapter 4

Data-driven control of DC-DC converters

In this chapter we continue the study of discrete-time systems; we develop an approach to control systems where dynamical models are either not readily available or highly complex in terms of equations and/or the amount of state variables. We thus resort to a data-driven paradigm which consists in using periodic measurements to approximate a dynamic model, which is then subjected to a control strategy. We endeavor to test such a control strategy operating on a boost converter under various increasingly complex scenarios, both theoretical and experimental, in order to properly verify the accuracy and plausibility of the entire data-driven approach. The following is an introduction to the fundamental concepts regarding the theory used to develop the main results.

4.1 Data suitability: Hankel matrix criteria

As previously discussed, we aim to develop a control strategy on a linearly approximated model. The process of generating such a model from sets of measured data is known as *system identification*. However, we must first examine some important conditions which determine whether the measured data are suitable for the analysis.

Notice that we endeavor to represent an unknown dynamical model; therefore, *sufficiency conditions* must be set to mathematically determine whether the data contain enough information about the model's dynamics. In order to define such conditions, we introduce the notion of a matrix constructed from data.

Consider a time series of length T expressed as $w(1), w(2), w(3), \dots, w(T)$, with $w : \mathbb{Z}_+ \rightarrow \mathbb{R}^q$ that corresponds to a set of measured data. A *Hankel matrix of depth L* , with $T \gg L \in \mathbb{Z}_+$ associated to this time-series is defined as

$$H_L(w) := \begin{bmatrix} w(1) & w(2) & \cdots & w(T-L+1) \\ w(2) & w(3) & \cdots & w(T-L+2) \\ \vdots & \vdots & \cdots & \vdots \\ w(L) & w(L+1) & \cdots & w(T) \end{bmatrix}. \quad (4.1)$$

Where T denotes the length of the time series, i.e., the amount of sampled data. As discussed in [33], the value of T must be high enough in order to guarantee optimal data quality and to increase the accuracy of the proposed system approximation. In practice, this is achieved by taking T to be “as long as possible” in order to mitigate the problem of *consistency*, i.e., the convergence of the identified system to the “true system”. Moreover, depth L is associated to the maximum order of the shift operator in the identified system and is required when determining further Hankel matrix properties associated with rank verification.

4.2 Classification of variables

Given a set of available system variables w , they can be classified as either *input* or *output* variables. Input variables are independent (e.g. duty cycle), while output variables are consequences of the inputs (e.g. output voltage). Such a concept is formalized below.

Given w that satisfies (3.2), the partition $w := \text{col}(u, y)$ is an *input/output partition* if

- 1) u is *free*, i.e., for all u there exists y such that $w = \text{col}(u, y)$.
- 2) u is *maximally free*, i.e., given u , no component of y is free.

If 1) and 2) hold, then u is called an *input variable* and y an *output variable*.

4.3 Persistency of excitation

Section 4.1 discussed the need to meet *sufficiency conditions* in order for a set of data to be considered suitable for analysis. One of these mathematical conditions is known as *persistency of excitation*, and implies that the measured input variable must exhibit an acceptable amount of variation over time. This is expressed formally in Theorem 4.1:

Theorem 4.1. “An input vector $u = u(1), u(2), \dots, u(T)$ is *persistently exciting* of order L if $H_L(u)$ is of full row rank.”

Persistency of excitation has the following important implication according to [33]. Recall that N denotes the maximum degree of a given linear difference system, and let

n be known as the *McMillan degree*, i.e. the smallest state space dimension among all possible state representations of (3.2). Given a time-series

$$w = w(1), w(2), w(3), \dots, w(T) := \text{col}(u, y) ,$$

that satisfies (3.2), if u is persistently exciting of at least order $N + n$, then $\text{colspan}(H_{N+n}(w))$ corresponds to the set of all possible solutions of (3.2). Therefore, the measured data is said to be *sufficiently informative*.

If the data is sufficiently informative, then a dynamical model of the system can be constructed from the set of available measurements $w(1), \dots, w(T)$ in the form of a linear difference system as described by equation (3.1). This implies that any admissible trajectory and behavior of w satisfying (3.2) can be recovered from such measured data.

4.4 Computation of coefficient matrices from data

As previously discussed, sufficiency of information implies that a given time series is suitable for analysis and control purposes. Moreover, such a time series can be used in the computation of the *left kernel*, or *nullspace*, of $H_L(w)$, i.e. a set containing a polynomial matrix $R(\sigma)$ such that $R(\sigma)w = 0$. This idea is formalized below.

Given $w = w(1), w(2), w(3), \dots, w(T) := \text{col}(u, y)$, a sufficiently informative time series that satisfies (3.2). There exists $\tilde{R} \in \mathbb{R}^{p \times (N+1)q}$ such that

$$\tilde{R} \begin{bmatrix} w \\ \sigma w \\ \vdots \\ \sigma^N w \end{bmatrix} = 0 ;$$

for all w that satisfies (3.2).

In order to compute such matrix \tilde{R} , we apply *singular value decomposition* (SVD) to the Hankel matrix [34]. For ease of reference, we recall the specifics behind SVD:

Consider $H_{N+1}(w)$, where N corresponds to the maximum degree of the shift operator. Using SVD, such a matrix can be *decomposed* (factorized) in the following way:

$$H_{N+1}(w) := U \Sigma V^T ;$$

where $U \in \mathbb{R}^{q \times q}$ and $V \in \mathbb{R}^{T \times T}$ are orthogonal, square matrices. Moreover, $\Sigma \in \mathbb{R}^{q \times T}$ is a diagonal matrix with nonnegative real values $\sigma_1 \geq \sigma_2 \geq \dots \geq \sigma_{\min} \geq 0$ on the diagonal. Notice that σ_i is known as the i -th *singular value* of Σ . Moreover, the number of nonzero singular values in the diagonal is determined by $r := \text{rank}(H_{N+1}(w))$. Thus, matrix Σ can be written as

$$\Sigma = \begin{bmatrix} \Sigma' & 0_{r \times (T-r)} \\ 0_{(q-r) \times r} & 0_{(q-r) \times (T-r)} \end{bmatrix} ,$$

where $\Sigma' \in \mathbb{R}^{r \times r}$ is a sub-diagonal matrix representing the set of nonzero singular values in the diagonal.

As previously discussed, singular value decomposition is of utmost importance in system identification theory since it provides a way to compute an *annihilator* of $H_{N+1}(w)$, i.e. its left kernel, a polynomial matrix $R(\sigma)$ such that (3.2) is satisfied. This idea is further formalized as follows.

Recall $w := \text{col}(u, y)$ and consider a Hankel matrix $H_{N+1}(w)$. Given a singular value decomposition $U\Sigma V^T$, consider the partition $U = \begin{bmatrix} U_1 & U_2 \end{bmatrix}$, where U_1 has r columns and U_2 has a $q - r$ number of columns equal to the number of outputs in w . Then, $\tilde{R} = U_2^T$ is the left kernel of $H_{N+1}(w)$. Note that matrix \tilde{R} contains sufficient information about the system dynamics based on the gathered data.

As a summary of the previously discussed ideas, we develop the algorithm depicted in Fig. 4.1, which shows how to perform the computation of the coefficient matrix \tilde{R} from a set of measured data.

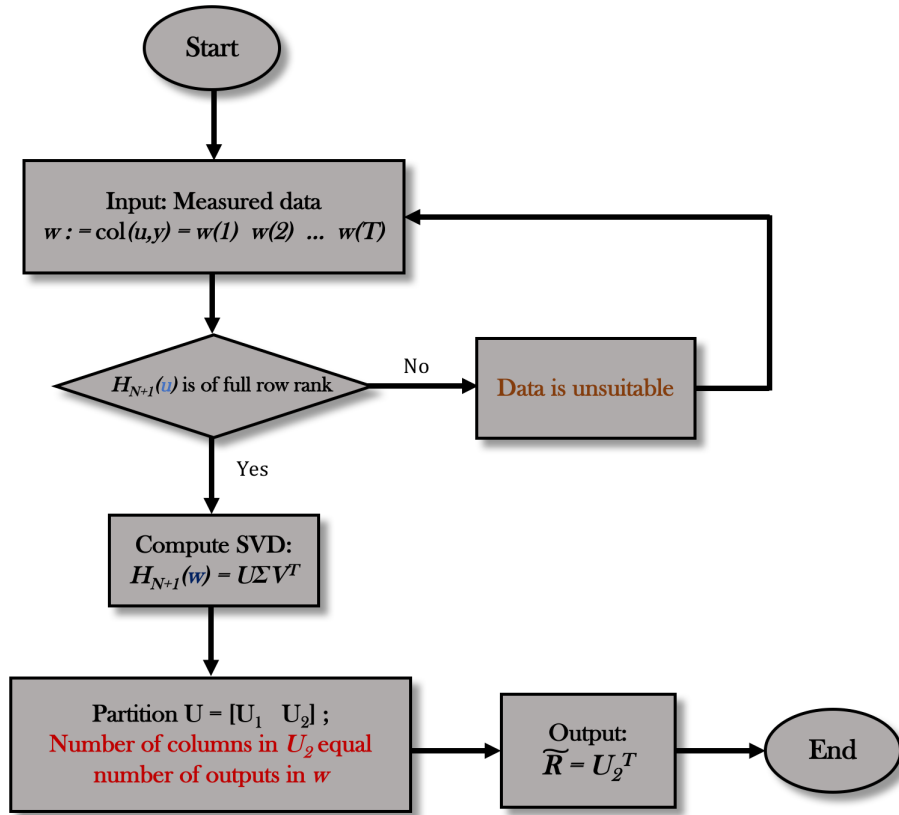


FIGURE 4.1: Algorithm for the computation of the coefficient matrix \tilde{R} from measurement data.

The following subsection shows how matrix \tilde{R} can be applied to the design of stabilizing controllers.

4.5 Control design purely from data

From Section 2.2.2, recall that we focus our efforts on studying system stability properties at the origin; therefore, we define *error variables* for each measured variable in a system. Namely, let $u : \mathbb{R} \rightarrow \mathbb{R}^m$ and $y : \mathbb{R} \rightarrow \mathbb{R}^n$ be the input/output variables. Particularly, in a boost converter, we recall that the input $u := d$ is the duty cycle while the output $y := \text{col}(i, v)$ contains the input current and output voltage. Thus, let $w := \text{col}(u, y)$ be the global set of variables of interest measured from a boost converter. The error variables for this set, denoted by \hat{w} , are defined by

$$\hat{w} := w - \bar{w} ;$$

where \bar{w} contains the values of the variable set at the fixed equilibrium. The following analogous notation for the input-output partition is used:

$$\hat{w} = \text{col}(\hat{u}, \hat{y}) .$$

Similar to the continuous-time control analysis studied in Section 2.3, when designing data-driven discrete controllers we do not impose a particular controller structure (P , PI , PID); instead, we adopt a general point of view for control design and let both the specific application and the data itself dictate the type of stabilizing controller to be used. Note that in this case, for ease of implementation we use a state space representation for the controller in a similar manner to the continuous case; however, these controllers also allow for higher-order representations due to the nature of the descriptions used in the discrete-time framework. Following these ideas, a feedback controller can adopt a general form

$$\begin{cases} \sigma z = Az + Bu' , \\ y' = Cz + Du' ; \end{cases} \quad (4.2)$$

where $z : \mathbb{R} \rightarrow \mathbb{R}^n$, $A \in \mathbb{R}^{n \times n}$, $B \in \mathbb{R}^{n \times m}$, $C \in \mathbb{R}^{k \times n}$, $D \in \mathbb{R}^{k \times m}$. In order to perform an interconnection between such a controller and a boost converter, let us define the controller input/output variables as the converter's output/input respectively; i.e., $u' := \hat{y}$ and $y' = \hat{u}$. This process, as well as the realization of the controller/converter combination, are depicted in Fig. 4.2.

Note that this controller admits any possible architecture (P , PI , PID) feedback configuration. Moreover, we resort to such a general point of view in accordance with our proposed line of study where we do not focus on a particular dynamical model; rather, we let the data invoke the requirements for stabilization.

Following this idea, the unknown model of the converter is thus considered as being represented by

$$R(\sigma)\hat{w} = 0 ;$$

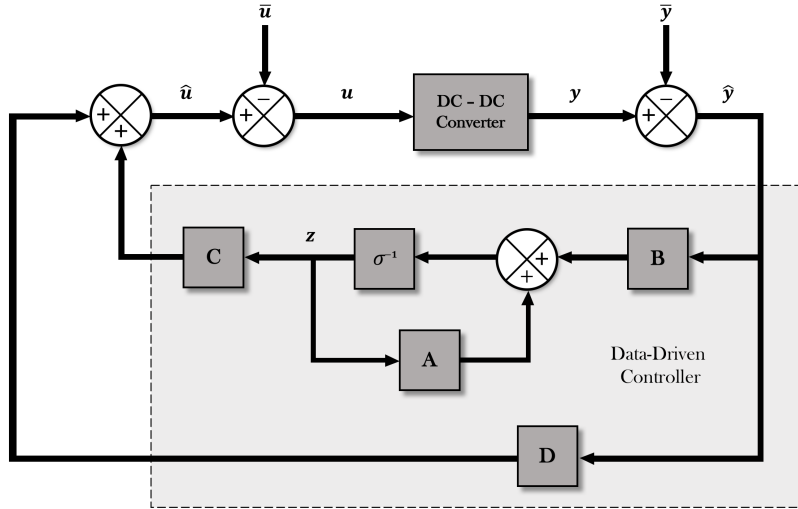


FIGURE 4.2: General realization of a data-driven feedback controller in state space form.

which can be congruently input-output partitioned as

$$\begin{bmatrix} R'(\sigma) & R''(\sigma) \end{bmatrix} \begin{bmatrix} \hat{u} \\ \hat{y} \end{bmatrix} = 0; \quad (4.3)$$

Let us now consider such a partition, as well as the controller equations in (4.2). Recalling that $u' := \hat{y}$ and $u' = \hat{y}$, then performing straightforward algebraic manipulation, yields the combined converter-controller model:

$$\underbrace{\begin{bmatrix} R'(\sigma) & R''(\sigma) & 0_{p \times n} \\ 0_{n \times k} & -B & \sigma I_n - A \\ I_k & -D & -C \end{bmatrix}}_{=: P(\sigma)} \begin{bmatrix} \hat{u} \\ \hat{y} \\ z \end{bmatrix} = 0. \quad (4.4)$$

From such a matrix, we can now obtain its coefficient matrix \tilde{P} as done in (3.8)-(3.9). Moreover, notice that coefficients \tilde{R} associated to $\begin{bmatrix} R'(\sigma) & R''(\sigma) \end{bmatrix}$ are directly obtained from the data and using the algorithm shown in Fig. 4.1.

Having obtained the combined converter-controller model, we recall that the stability conditions for linear difference systems established in section 3.3 can be applied to the combined model (4.8) in such a manner that a stable plant-converter interconnection can be mathematically established by solving the augmented version of the inequality previously described by (3.10):

$$\begin{bmatrix} 0_{r \times r} & 0_{r \times Nr} \\ 0_{Nr \times r} & K \end{bmatrix} - \begin{bmatrix} K & 0_{Nr \times r} \\ 0_{r \times Nr} & 0_{r \times r} \end{bmatrix} + \tilde{P}^\top \tilde{Y} + \tilde{Y}^\top \tilde{P} < 0; \quad (4.5)$$

where the controller parameters A , B , C and D (commonly known as *gains*) which are now embedded in \tilde{P} , are unknown; $r := q + k + m + n$ is a matrix dimension parameter, and N denotes the maximum lag in the discrete system.

Since parameters of both \tilde{P} and \tilde{Y} are unknown, condition (4.5) is, in general, a *bi-linear matrix inequality (BMI)*, for which solutions can be found by standard iterative algorithms (see Fig. 2.8).

4.6 Gain computation

The general converter-controller structure in (4.4) allows us to design controllers without imposing a particular control scheme, but instead letting the specific application be the determining factor for such a decision. For instance, let us consider the particular case of a commercial boost converter whose manufacturer's pre-defined controller only allows for gain modification and is comprised by a double loop current-voltage nested controller, as depicted in Fig. 4.2.

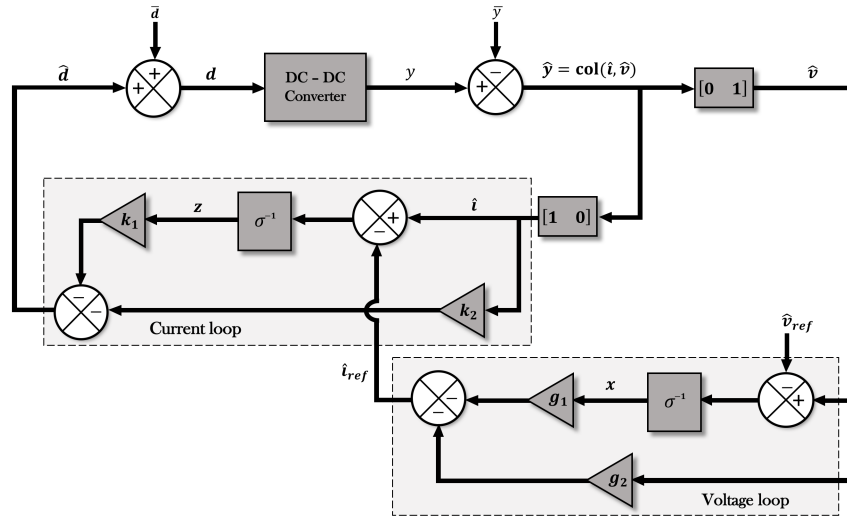


FIGURE 4.3: Predefined feedback controller example.

Defining the converter error variables as $\hat{w} = \text{col}(\hat{d}, \hat{y})$ with $\hat{y} = \text{col}(\hat{i}, \hat{v})$, then the proposed controller equations can be written as follows:

$$\text{Voltage loop: } \begin{cases} \sigma x = x + \hat{v} - \hat{v}_{ref} , \\ \hat{i}_{ref} = -g_1 x - g_2 \hat{v} ; \end{cases} \quad (4.6)$$

$$\text{Current loop: } \begin{cases} \sigma z = z + \hat{i} - \hat{i}_{ref} , \\ \hat{d} = -k_1 z - k_2 \hat{i} ; \end{cases} \quad (4.7)$$

where $\phi, z : \mathbb{Z}_+ \rightarrow \mathbb{R}$ and $k_i, g_i, i = 1, 2$, are scalar quantities known as *gains*. Given this set of equations and considering the unknown converter model

$$\begin{bmatrix} R'(\sigma) & R''(\sigma) & R'''(\sigma) \end{bmatrix} \begin{bmatrix} \hat{d} \\ \hat{i} \\ \hat{v} \end{bmatrix} = 0 ,$$

we can construct the augmented model

$$\underbrace{\begin{bmatrix} R'(\sigma) & R''(\sigma) & R'''(\sigma) & 0_{p \times 1} & 0_{p \times 1} \\ 1 & k_2 & 0 & k_1 & 0 \\ 0 & -1 & -g_2 & \sigma - 1 & -g_1 \\ 0 & 0 & -1 & 0 & \sigma - 1 \end{bmatrix}}_{=:P(\sigma)} \begin{bmatrix} \tilde{d} \\ \hat{i} \\ \hat{v} \\ x \\ z \end{bmatrix} = 0. \quad (4.8)$$

Then controller gains k_1, k_2, g_1 and g_2 , which guarantee converter stability, can be computed using (4.5) by means of standard LMI solvers such as `Yalmip` [27].

4.7 Results

Simulations and experimental tests were carried out in order to validate the above theoretical achievements. By means of the numerical environment `MATLAB`, we write computer algorithms to perform computations where needed. Moreover, we simulate circuits using the power electronics software `PSIM`. Finally, we carry out an experimental setup in order to demonstrate the application of data-driven control theory on a tangible, dynamically complex system.

4.7.1 Control of DC-DC converter with nominal resistive load

Using the predefined controller structure depicted in Fig. 4.3, we first test the data-driven control strategy on a traditional boost converter with a resistive load and the nominal parameters shown in Table 4.1.

TABLE 4.1: *Nominal parameters for simulation.*

<i>Notation</i>	<i>Parameter description</i>	<i>Value</i>
V_{in}	<i>Input voltage</i>	50V
\bar{V}	<i>Output voltage at equilibrium</i>	100V
L	<i>Inductor</i>	300 μ H
C	<i>Capacitor</i>	10 μ F
R	<i>Load resistance</i>	50 Ω
h	<i>Time step for numerical method</i>	1 μ s
f_s	<i>Transistor switching frequency</i>	50kHz

Using the averaged boost converter model, it is easy to verify the equilibrium values for the proposed circuit to be

$$\bar{d} = \frac{\bar{v} - v_{in}}{\bar{v}} = 0.5 ; \quad \bar{i} = \frac{\bar{v}}{R} \left(\frac{1}{1 - \bar{d}} \right) = 1 \text{ A} .$$

Recall from section 4.3 that one of the principles behind data-driven control is persistency of excitation. Thus, in order to gather sufficiently informative data from the to-be-controlled system, we generate an arbitrary custom sinusoidal waveform to act as the input d , shown in Fig. 4.4.

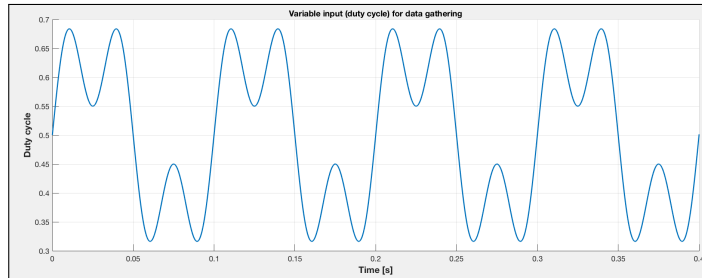


FIGURE 4.4: Varying input signal.

For reference, note that such a waveform is described by the following expression:

$$d = 0.1 \sin(60\pi t) + 0.15 \sin(20\pi t) + 0.5 .$$

A PSIM schematic depicting the previously described boost converter with the proposed variable input is shown in Fig. 4.5.

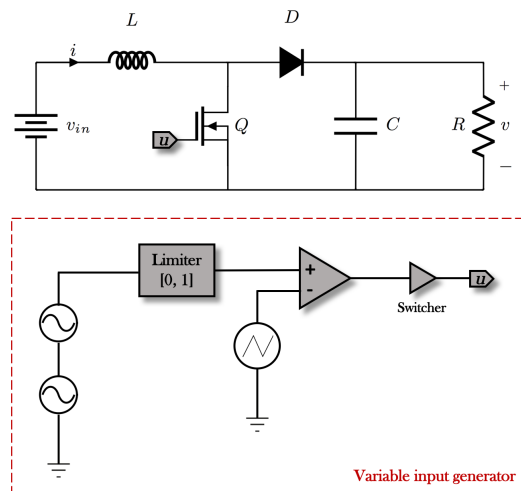


FIGURE 4.5: Boost converter with variable input used to gather data.

Notice that the sole purpose of this circuit is to provide sufficiently informative data to be processed with the algorithm shown in Fig. 4.1, whose goal is to approximate an unknown dynamic model. Fig. 4.6 shows the circuit response; as expected, the variable input causes an unstable voltage behavior which allows for data gathering and further processing.

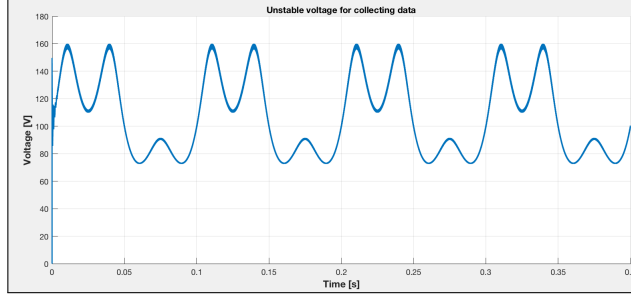


FIGURE 4.6: Unstable voltage response for data gathering.

Such data, as well as corresponding current and duty cycle values, are expressed as a time series $w := w(1) w(2) \cdots w(T)$ and converted to error variables, i.e. $\hat{w} = w - \bar{w}$, which are used as the input to the aforementioned algorithm. Thus, coefficient matrix \tilde{R} is numerically computed and represented as:

$$\tilde{R} := \underbrace{\begin{bmatrix} 0.7281 & -0.0154 & -0.0001 & 0.6846 & 0.0305 & -0.0074 \\ 0.6840 & -0.0207 & -0.0001 & -0.7289 & 0.0201 & 0.0004 \end{bmatrix}}_{:= [R_0 \mid R_1]}; \quad (4.9)$$

which corresponds to the coefficient matrix of a linear difference system with lag $N = 1$. Such a matrix is then embedded into the augmented converter-controller model described by (4.8), obtaining matrix \tilde{P} to be used in the stability condition (4.5). Finally, the LMI of such a condition is solved, yielding the following gain values:

$$k_1 := 0.0065; \quad k_2 := 0.0343; \quad g_1 := 0.0008; \quad g_2 := 0.0011.$$

Using these gains, the proposed control circuit is implemented by means of the Control toolbox in PSIM and is shown in Fig. 4.7. Notice that such a circuit is built in accordance with the proposed pre-defined control structure, i.e., Fig. 4.3. Moreover, the equilibrium values and reference constants for the error variables \hat{w} are represented by blank boxes in the summation points. Finally, notice that the circuit output is a value for the duty cycle d . However, we translate such a value into a switching signal for the active switch by means of a classic PWM generator, which consists of a comparator with a 50 kHz, 1 V_{peak} triangular waveform.

Results of the circuit subjected to the proposed control strategy are depicted in Fig. 4.8. As expected by design, the data-driven controller is able to regulate the output voltage at the desired equilibrium value.

In order to further test the controller's performance, we induce a +10V step in the input voltage starting at $t = 0.4s$. We show the response to this disturbance in Fig. 4.9. Notice that the controller is able to robustly maintain the output at a desired value regardless of abrupt changes to the input voltage.

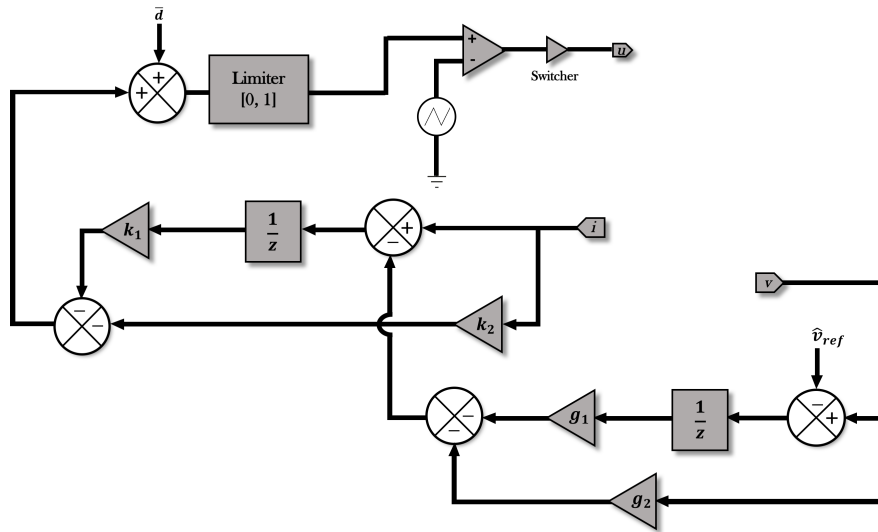


FIGURE 4.7: Control circuit implemented in PSIM.

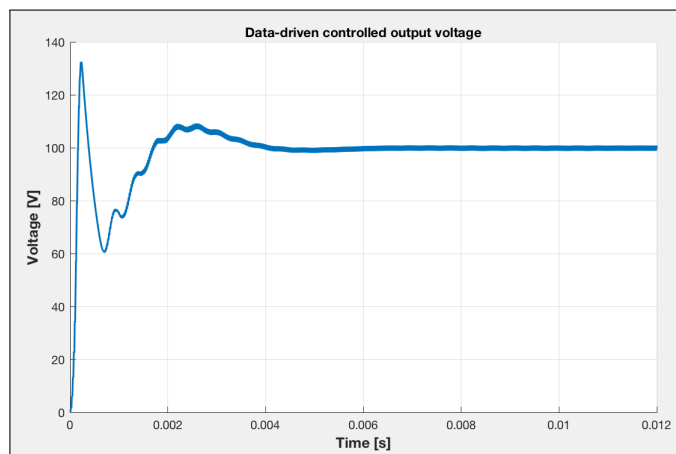


FIGURE 4.8: Circuit response to data-driven controller.

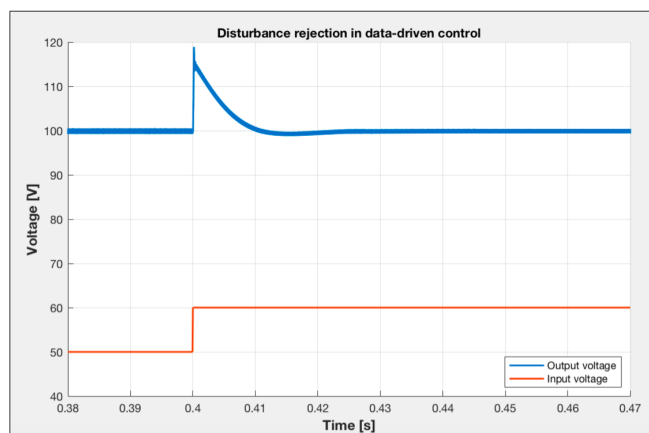


FIGURE 4.9: Disturbance rejection at time step $t = 0.4s$.

4.7.2 Control of DC-DC converter with DC machine load

As a further proof of concept regarding the data-driven control scheme, consider the circuit in Fig 4.10, consisting of the same boost converter as the previous section (please refer to Table 4.1 for nominal parameters of converter) but with a different type of load. In this case, the armature winding of a separately excited DC machine with a nominal load torque (please refer to Table 4.2 for parameters) is placed at the output of the converter. Notice that in order to derive the equations for this new system, several new state variables would need to be taken into account; this would imply a notable increase in complexity regarding the new model. Moreover, there is no deterministic approach to the modeling of the load torque. Motivated by such issues, we resort to a data-driven control strategy which can guarantee asymptotic stability without the need to consider mathematically complex scenarios.

TABLE 4.2: DC machine parameters.

Notation	Parameter description	Value
V_a	Induced armature voltage	150V
R_a	Armature winding resistance	6.5Ω
i_a	Field winding current	0.45A
L_{af}	Mutual inductance	65mH
J	Rotor moment of inertia	0.005kg/m ²
B_L	Viscous friction coefficient	0.5

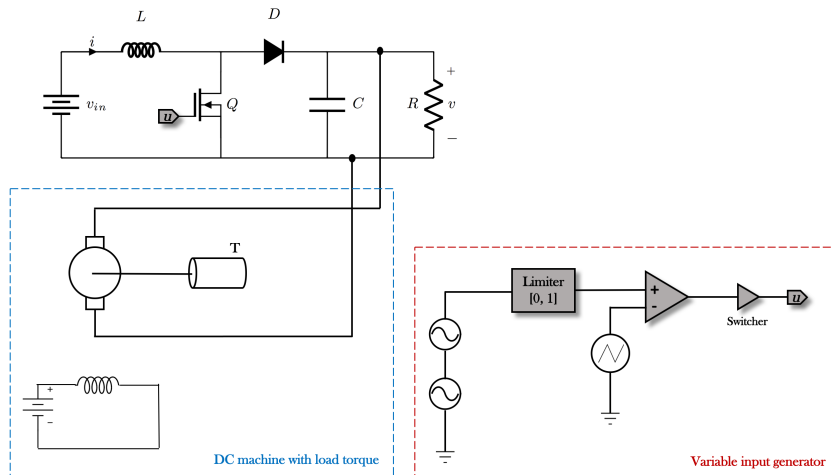


FIGURE 4.10: Boost converter with DC machine load.

Notice that the variable input, necessary for persistency of excitation to be fulfilled, is the same signal as in the previous case, i.e. Fig. 4.4. Similarly, the corresponding unstable output voltage is shown in Fig. 4.11.

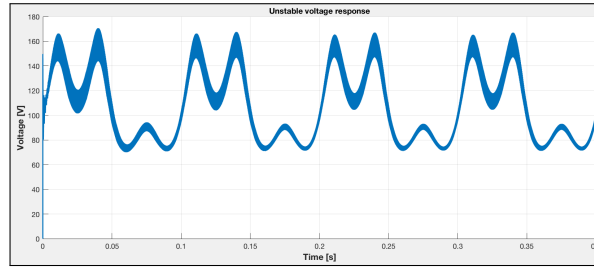


FIGURE 4.11: Unstable voltage response for data gathering in DC machine-loaded circuit.

As in the previous case, such a signal along with current and duty cycle are taken as data and placed in a time series $w := w(1) w(2) \cdots w(T)$, whose elements are then converted to error variables i.e. $\hat{w} = w - \bar{w}$ and used as the input to the algorithm in Fig. 4.1. Thus, coefficient matrix \tilde{R} is numerically computed and represented as:

$$\tilde{R} := \underbrace{\begin{bmatrix} -0.2489 & -0.0037 & 0.0122 & 0.0278 & -0.0017 & -0.6750 & 0.2579 & 0.0003 & 0.6442 \\ -0.6167 & -0.0082 & 0.0330 & -0.0649 & -0.0054 & 0.2310 & 0.6973 & -0.0026 & -0.2733 \end{bmatrix}}_{:= [R_0 \mid R_1 \mid R_2]};$$

which corresponds to a linear difference system with lag $N = 2$. Matrix \tilde{R} is then substituted into the converter-controller augmented model described by (4.8). Thus, such a model's coefficient matrix \tilde{P} is used in order to solve the stability condition in (4.5) using `Yalmip`. This computation yields the following controller gains:

$$k_1 := 0.0045; \quad k_2 := 0.0175; \quad g_1 := 0.0142; \quad g_2 := 0.0827.$$

Consequently, these gains are used as parameters in the control circuit shown in Fig. 4.7, whose output is fed to the boost converter as a variable duty cycle. Shown below in Fig. 4.12 are the results of the proposed control strategy; as expected, the output voltage is robustly regulated at the desired equilibrium point despite abrupt changes at the input voltage, namely a +10 V step added at time instant $t = 0.3$ s.

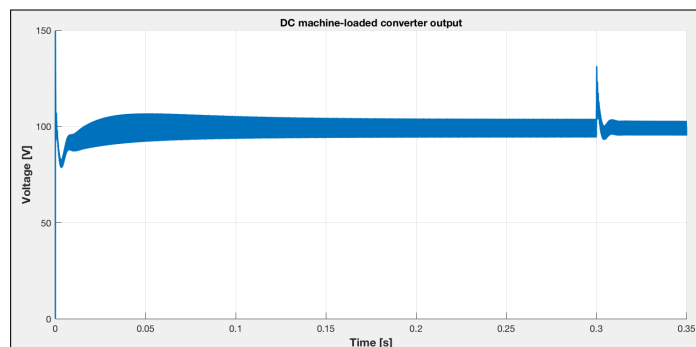


FIGURE 4.12: Controlled voltage of a Boost converter with DC machine load.

Additionally, Fig. 4.13 shows the input current being regulated. Note that, at the aforementioned time instant where the disturbance is induced, the current moves to a

new equilibrium value; this is as expected by the fact that the double-loop controller ensures that the reference current –that maintains the output voltage at a constant value– is a function of the output voltage variable.

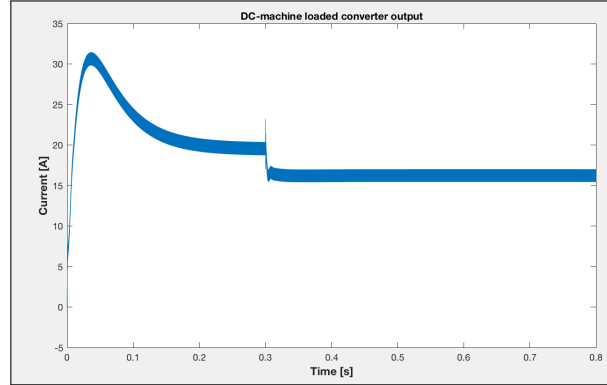


FIGURE 4.13: Controlled current in Boost converter.

4.7.3 Experiment: Control of DC-DC converter with constant power load (CPL)

We now endeavor to experimentally validate our proposed data-driven control strategy on two conventional boost converters, one of them operating as a constant power load (CPL). Note that such DC-DC converter interconnections are a common occurrence in energy distribution networks. However, from electronics theory, we recall that feeding an individually controlled boost converter with a nonlinear load causes instability. Moreover, there remains the issue of dealing with increasingly complex mathematical models which we become unable to describe using conventional tools and representations. Thus, we resort to a data-driven control strategy in an attempt to mitigate the aforementioned issues and, most fundamentally, guarantee asymptotic stability in the entire network-interconnected model.

The proposed circuit diagram is shown in Fig. 4.14, part of which consists of a traditional boost converter (known as “source”) with duty cycle d , input current i , output voltage v , and output current I_o . The source converter does not have a nominal load at the output; rather, a second boost converter (known as “constant power load (CPL)”) is connected as a load.

Note that the source converter’s output variables are considered as inputs to the CPL; i.e., the latter’s available variables are comprised of input voltage v , input current I_o and duty cycle u .

As previously discussed, the main contribution in this section is the development and testing of prototypes which endeavor to validate the data-driven control material presented in this chapter. We thus choose to implement the CPL case discussed in this subsection. To such purpose, we build two separate boost converters (source and load)

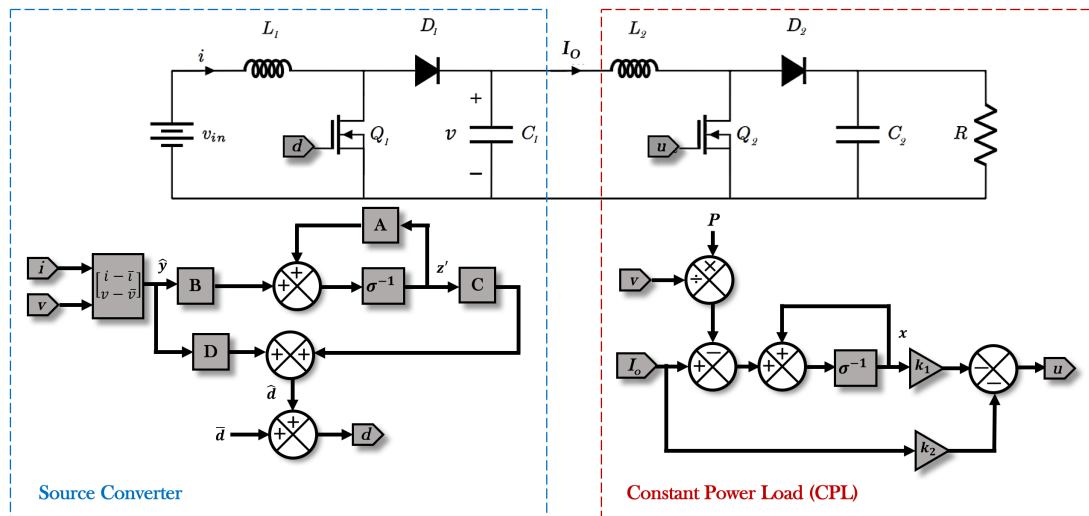


FIGURE 4.14: Source and load converters and corresponding controllers.

using the nominal parameters shown in Table 4.3. Photographic evidence of the experimental testbed is depicted in Fig. 4.15. Controllers are implemented by means of a DSP card TI28335, acquiring signals from both voltage and current sensors at 10 kHz. However, the transistor switching frequency is fixed at 50 kHz. Moreover, the load converter delivers constant power to an electronic load BK-8616.

TABLE 4.3: Data of the experiment

Notation	Parameter	20cm Value/Part
v_{in}	Input voltage (changes)	25V, 30V, 35V
\bar{v}_C	Equilibrium voltage (Source converter)	60V
L_1, L_2	Inductors 1 and 2	240 μ H
C_1, C_2	Capacitors 1 and 2	10 μ F
S_1, S_2	MOSFETs 1 and 2	IRFP264pbf
D_1, D_2	Diodes 1 and 2	MBR40250G
R	Resistor (Electronic load)	150 Ω
f_s	Sampling frequency (controller)	10kHz
f_c	Transistor switching frequency	50kHz
k_1, k_2	Gains of CPL loop control	0.0039, 0.0099

Based on this setup, we perform three main experiments in order to show:

1. The standalone performance of the source converter with a nominal resistive load;
2. Such a converter's unstable, degraded behavior when connected to a CPL instead of a nominal load;

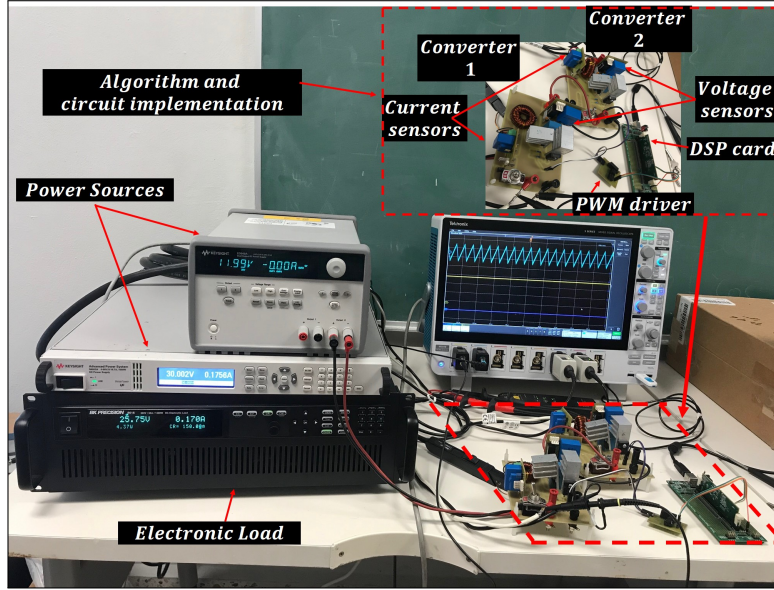


FIGURE 4.15: Experimental setup.

3. The stabilization of both interconnected converters using a data-driven control strategy.

As a preamble of the main contribution, we implement a controller with an optimal performance and disturbance rejection capabilities, i.e., we test a *standalone* closed-loop design on a tangible converter prototype considering a nominal resistive load of 24Ω . A traditional linear controller, such as the one described by (4.6) - (4.7), is implemented with the following gain values:

$$k_1 := 0.0045 ; k_2 := 0.0112 ; g_1 := 0.0056 ; g_2 := 0.0301 .$$

Shown in Fig. 4.16 is the circuit's closed-loop response under abrupt changes at the input voltage (please see Table 4.3 for details). As expected, the response is asymptotically stable and the output voltage is robustly regulated despite the aforementioned disturbances.

As per point 2) of the experiment list, we now replace the nominal resistive load by a CPL (load converter) extracting as much power from the source converter as the previous nominal load, i.e. $P = 150 W$. In order for this value to remain constant, the CPL's *input current* must satisfy the following nonlinear algebraic equation:

$$I_o = \frac{P}{v} .$$

Such a current is tracked by the current controller depicted in the right-hand side of Fig. 4.14, with gain values defined as $k_1 := 0.0039$, $k_2 := 0.0099$.

Shown in Fig. 4.17 is the source converter's output voltage subjected to the same control strategy as in the standalone case. Notice that such a behavior is oscillatory,

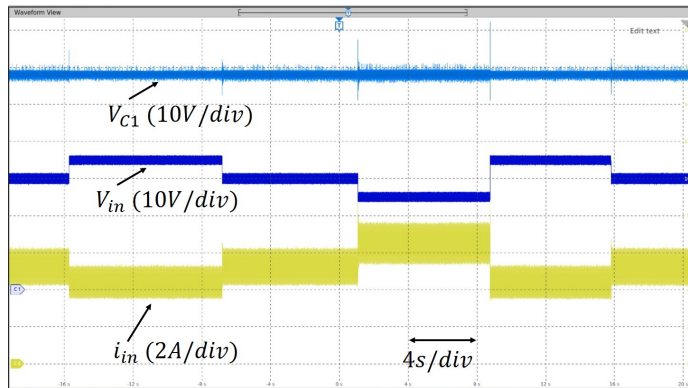


FIGURE 4.16: Input current i_{in} and output voltage v_{C1} behavior under abrupt changes at the input voltage v_{in} .

i.e. unstable; this is deemed unacceptable for practical implementations, since the DC bus exhibits a low quality energy profile. Hence, this experiment illustrates the well-known problem of instability in interconnected power converters (see [6, 21–24]). Namely, individual closed-loop converters become unable to regulate their output voltage when it is connected to a CPL, which implies a degraded performance. Moreover, the complexity of the interconnected source-CPL dynamics implies that traditional model-dependent control schemes are rendered difficult to use in such a case.

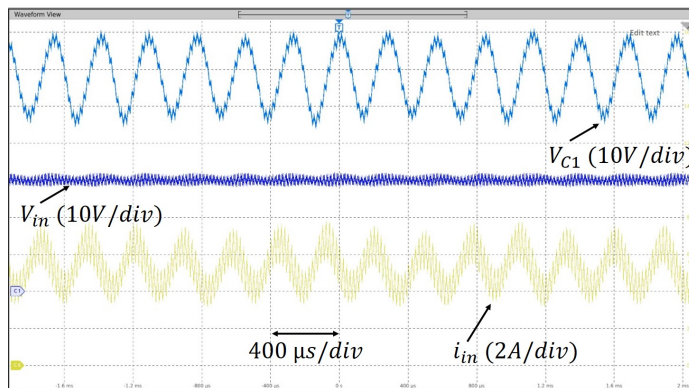


FIGURE 4.17: Instability in the source converter produced by the connection of a constant power load.

Motivated by the aforementioned ideas and as per point 3) of the experiment list, we propose a data-driven stabilizing control strategy. For ease of implementation, we use the data provided in Fig. 4.17; such an option becomes plausible when we notice that the system's naturally unstable behavior satisfies the persistency of excitation condition. This, in turn, implies that the data is sufficiently informative for us to process and use in system identification. As such, we build data vectors $\hat{w} = \text{col}(\hat{d}, \hat{i}, \hat{v})$ from the unstable converter response in order to run the algorithm in Fig. 4.1 and to solve inequality (4.5) using Yalmip. Such a process yields the following new stabilizing gains:

$$k_1 := 0.0022 ; k_2 := 0.0278 ; g_1 := 0.0028 ; g_2 := 0.1441 .$$

The controller shown in the left-hand side of Fig. 4.14 is thus implemented. For ease of reference, we recall its equations:

$$\begin{cases} \sigma z' = Az' + B\hat{y}, \\ \hat{d} = Cz' + D\hat{y}; \end{cases} \quad (4.10)$$

where $z' : \mathbb{R} \rightarrow \mathbb{R}^q$ is a vector containing q number of controllers. Thus, recalling the structure of the proposed double-loop controller described by (4.6) - (4.7), it follows that (4.10) is merely a state space representation of (4.6) - (4.7) where $z' := \text{col}(z, \phi)$ and, evidently, $q = 2$. As such, the corresponding coefficient matrices are defined as

$$A := \begin{bmatrix} 1 & 0.0028 \\ 0 & 1 \end{bmatrix}; \quad B := \begin{bmatrix} 1 & 0.1441 \\ 0 & 1 \end{bmatrix}; \\ C := \begin{bmatrix} -0.0022 & 0 \\ 0 & 0 \end{bmatrix}; \quad D := \begin{bmatrix} -0.0278 & 0 \\ 0 & 0 \end{bmatrix}.$$

Shown in Fig. 4.18 are the results of this test. We start the experiment from the originally unstable behavior caused by the previous controller, then switch into a data-driven strategy which reformulates the gains and steers the output voltage into a stable behavior with minimum oscillation. Moreover, due to the stabilization of the source converter's output voltage, the CPL's input current I_o is now constant; therefore, it follows that the CPL's output voltage v_{C_2} will behave in a stable manner as well.

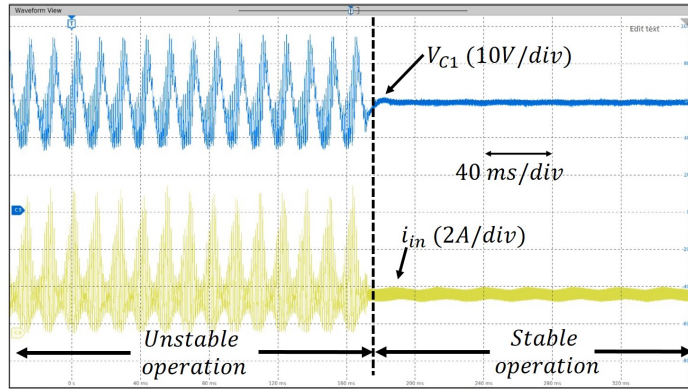


FIGURE 4.18: Source converter's input current i and output voltage v stabilization derived from modifying the control strategy.

4.7.4 Data-driven multi-controller system

As done in Section 2.5.3 with the continuous-time case, we now endeavor to test the multi-controller strategy applied to the data-driven control strategy developed in this chapter. Although the main motivation and theoretical details surrounding the use of multi-controller systems are explained thoroughly in Section 2.4, for ease of reference we recall the fundamentals of such material.

Consider a converter-controller combined model, such as the one described by (4.8). This augmented model's coefficient matrix \tilde{P} can be substituted in condition (4.5) in order to compute stabilizing controller gains. By noticing that such a condition is an *inequality*, it becomes evident that multiple solutions (stabilizing gain sets) can be computed, each one inducing a different dynamic profile on the controlled system's behavior. These multiple profiles, or scenarios, can be *switched into* depending on some arbitrarily imposed condition. Recall that we impose this condition to be

$$\|E(5nT) - E(5(n-1)T)\| \leq \epsilon,$$

whose parameters are defined and explained in (2.18). Moreover, for ease of reference, a graphical depiction of the logic behind multi-controller systems is given by Fig. 2.5.

Following these ideas, consider the traditional boost converter subjected to a data-driven control strategy in Section 4.7.2 We calculate multiple stabilizing gains for this converter, thus generating a "bank" of controllers, by using the linearization algorithm shown and explained in Fig. 2.8. Note that we have developed such theory for continuous-time systems; however, the existing analogy between continuous-time and discrete-time systems allows us to easily adapt the material from one domain to the other. Therefore, Fig. 4.19 shows a discrete-time version of the algorithm which now considers matrix \tilde{P} and inequality (4.5).

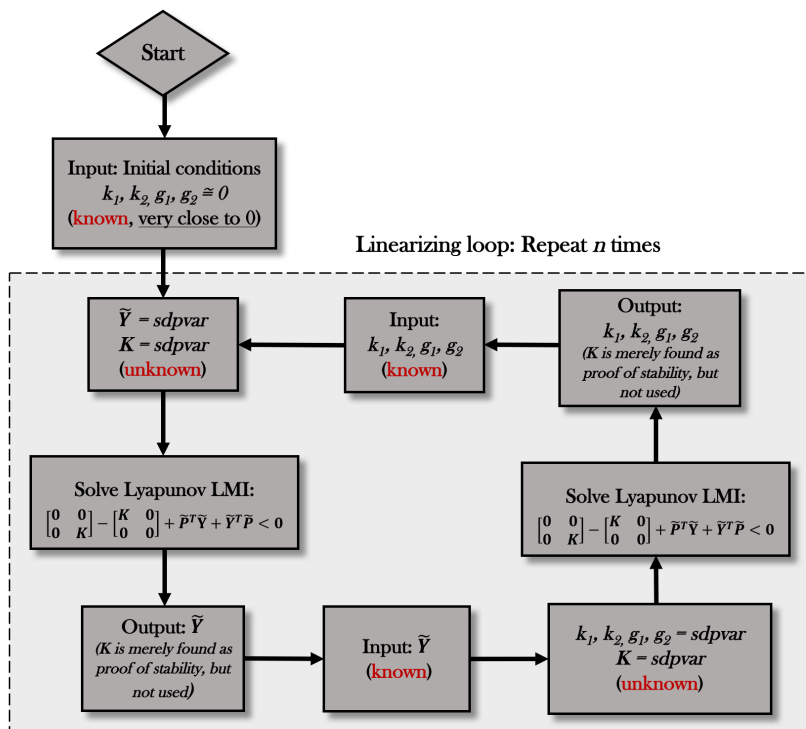


FIGURE 4.19: Discrete-time algorithm for controller bank generation.

The aforementioned traditional boost converter, whose parameters are detailed by Table 4.1, has an associated coefficient matrix \tilde{R} shown in (4.9). Such a matrix is embedded

in the augmented model (4.8), thus forming matrix \tilde{P} to be used in the controller bank algorithm.

Starting such an algorithm with initial conditions

$$k_1 := 0.001 ; \quad k_2 := 0.0001 ; \quad g_1 := 0.0001 ; \quad g_2 := 0.0001 ,$$

for an arbitrary $n = 40$, we generate the gain matrix \mathfrak{C}_{40} (see Section 2.5.3 for details) in table form, shown in Fig. 4.20.

Row	k_1	k_2	g_1	g_2
1	0.0001	0.0008	0.0188	0.2748
2	0.0003	0.0031	0.0232	0.5166
3	0.0006	0.0073	0.0236	0.5036
4	0.0007	0.0083	0.0240	0.4985
5	0.0009	0.0095	0.0250	0.4916
6	0.0012	0.0119	0.0249	0.4919
7	0.0013	0.0140	0.0250	0.4921
8	0.0013	0.0134	0.0253	0.4917
9	0.0018	0.0134	0.0358	0.5198
10	0.0018	0.0139	0.0356	0.5192
11	0.0021	0.0154	0.0369	0.5161
12	0.0021	0.0146	0.0370	0.5147
13	0.0021	0.0144	0.0361	0.4721
14	0.0026	0.0162	0.0363	0.4737
15	0.0030	0.0164	0.0387	0.4912
16	0.0030	0.0166	0.0377	0.4796
17	0.0039	0.0176	0.0472	0.5385
18	0.0041	0.0173	0.0517	0.5609
19	0.0039	0.0166	0.0508	0.5511
20	0.0042	0.0164	0.0501	0.5058
21	0.0049	0.0162	0.0517	0.5197
22	0.0049	0.0158	0.0528	0.5315
23	0.0056	0.0167	0.0545	0.5406
24	0.0059	0.0161	0.0550	0.5581
25	0.0060	0.0162	0.0544	0.5730
26	0.0061	0.0159	0.0564	0.5485
27	0.0063	0.0161	0.0545	0.5425
28	0.0063	0.0162	0.0565	0.5442
29	0.0062	0.0159	0.0555	0.5469
30	0.0062	0.0157	0.0558	0.5445
31	0.0071	0.0175	0.0564	0.5516
32	0.0075	0.0170	0.0656	0.5833
33	0.0076	0.0171	0.0662	0.5765
34	0.0075	0.0171	0.0653	0.5789
35	0.0077	0.0169	0.0648	0.5825
36	0.0074	0.0165	0.0636	0.5613
37	0.0077	0.0173	0.0636	0.5628
38	0.0085	0.0187	0.0636	0.5793
39	0.0086	0.0188	0.0642	0.5866
40	0.0086	0.0187	0.0643	0.5969

FIGURE 4.20: Stabilizing controller bank for $n = 40$.

As in the continuous-time case, notice that the gain values exhibit a linear convergence to an unknown value as we repeatedly solve the gain computation algorithm. However, unraveling such a value is not the focus of this analysis; rather, we benefit from the fact that this process generates asymptotically stable gains for the converter-controller interconnection.

Consider the to-be-controlled boost converter, whose nominal parameters are shown in 4.1 and whose diagram is shown in Fig. 2.1. Using PSIM, we carry out a simulation of the multi-controller strategy with a maximum switching threshold error of $\epsilon = 1$, as well as the following *desired trajectory*:

$$y^*(t) = 80[1 - e^{-1000t} \cos(700t)] .$$

Shown in Fig. 4.21 is the control circuit implementing the multi-controller strategy. Note that this diagram is similar in structure to the one used in previous simulations (see Sections 4.7.1 and 4.7.2), differing mainly in the addition of *C Blocks* in order to implement modules corresponding to desired trajectory generation, switching condition implementation and controller switching execution. Such modules are programmed by means of input-output oriented C language. Classic programming structures, e.g. arrays, were also used in the C Blocks in order to include the controller bank shown in Fig. 4.20.

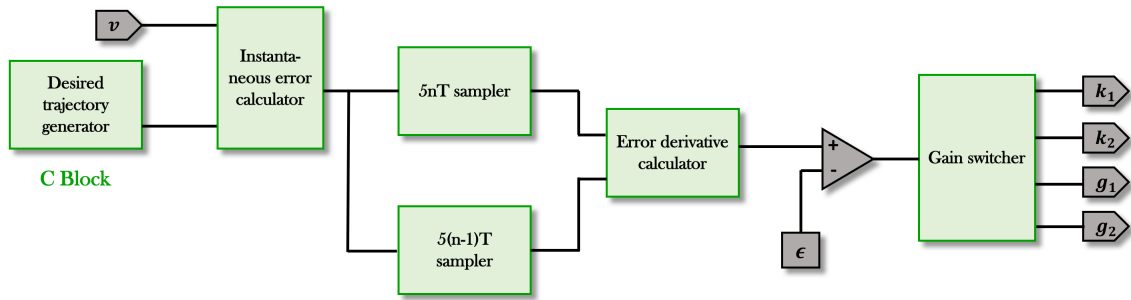
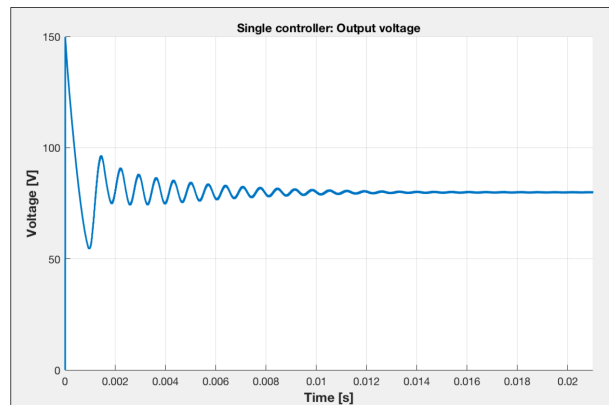
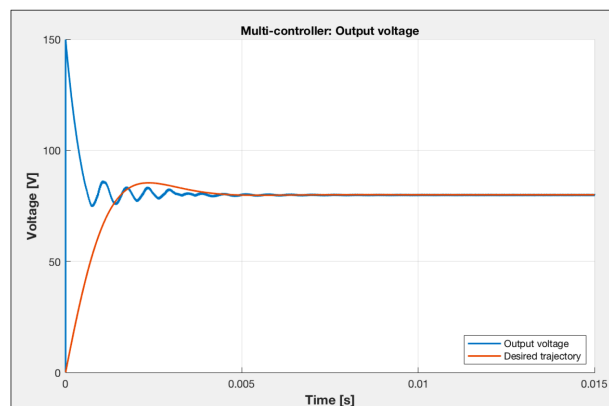


FIGURE 4.21: Multi-controller strategy implemented in PSIM.

Fig. 4.22 (a) shows the circuit's response when controlled using only one set of gains from the gain matrix. In contrast, Fig. 4.22 (b) shows the response when the converter is subjected to the proposed multi-controller method. Note that the "real trajectory" is colored red, whereas the desired trajectory is colored blue. Notice that the multi-controller strategy causes a slightly perceptible improvement in response time with respect to the single-controller response. Moreover, the multi-controller strategy steers the output "as close as possible" to the desired trajectory within the allowed threshold ϵ .



(a)



(b)

FIGURE 4.22: Output behavior with (a) a single controller, (b) the multi-controller strategy.

Chapter 5

Conclusions and future work

We proposed a model-less approach to DC-DC power converter control based purely on data, using concepts of discrete-time system analysis such as behavioral system theory, system identification and Lyapunov stability criteria. Moreover, we developed a multi-controller framework which, according to specific performance conditions, switches into different sets of controllers in order to robustly regulate the output dynamics to a desired behavior. In the following, we summarize the material covered in this thesis.

Chapter 2:

- We introduced the concept of *average modeling*, which is an instrumental element in both linear and nonlinear power converter analysis. We discussed that averaging involves modeling a converter's equivalent topologies when the switching input is on, i.e. $u = 1$, and when it is turned off, i.e. $u = 0$. Such a binary input variable is then replaced by the *duty cycle* which is, intuitively, an *average* input variable acting over a *switching time period*.
- We discussed *linearization* and argued that the use of linear feedback controllers to regulate nonlinear converters is an appropriate choice due to their single equilibrium point. Therefore, by using first degree Taylor series expansion and defining *error variables*, we developed a linearized model of a boost converter from which stabilizing controllers were to be synthesized.
- A general framework for converter-controller interconnections was given. We discussed that such interconnections produce *augmented* state-space representations, for which stabilizing controller gains can be computed by using *Lyapunov criteria* and finding solutions to an LMI.
- We developed an algorithm for the generation of a switching multi-controller system using gains from a *gain matrix* (or *controller bank*), benefitting from the fact that the linearization of the Lyapunov criteria provides us with multiple solutions

to an LMI. We showed that a switching controller framework induces robustness and endeavors to steer the output dynamics into the best-performing profile available.

- We carried out simulations as a proof of concept; we showed that boost converters can be stabilized with gains computed from Lyapunov criteria. We also discussed that the switching multi-controller strategy is able to steer the dynamics as close as possible to a desired trajectory, inducing notable improvements in the transient response.

Chapter 3:

- We switched the focus of study to discrete-time systems, establishing an analogy between continuous-time and discrete-time representations; namely, we introduced *linear difference systems* as a way to model systems of order N .
- We established *quadratic difference forms* as the means to study stability properties in linear differential systems.
- Further analysis regarding Lyapunov criteria has been given; we developed a discrete-time version of the augmented inequality established in Chapter 2. As such, we showed that by using a system's coefficient matrix \widetilde{R} , the Lyapunov inequality provides information about system stability based on quadratic difference forms.

Chapter 4:

- We discussed the possibility of controlling systems whose model is either highly complex or not readily available; to such purpose, we introduced the concept of *Hankel matrices*, which are matrices constructed from a set of data. We argued that the use of such matrices is fundamental in what is known as *system identification*, i.e., the process of recreating a previously unknown model using only measured data from the system.
- We introduced the concept of *persistency of excitation* as a condition for the measured data to be *sufficiently informative* about the to-be-recreated model's dynamics. We showed that the rank of a Hankel matrix plays an important role in verifying such a condition, and that sufficiency of information implies the possibility of computing the unknown system's coefficient matrix.
- We developed an algorithm for the computation of an unknown system's coefficient matrix. Given a sufficiently informative set of data, we showed that its associated Hankel matrix can be factorized using *singular value decomposition*. Such a technique allows us to obtain coefficient matrix \widetilde{R} in a straightforward manner.

- We developed a discrete-time counterpart to the augmented state space representation developed in Chapter 2. Using higher-order representations with the recreated model's coefficient matrix \tilde{R} as a parameter, we create a converter-controller interconnection matrix from which stability properties can be determined.
- We created a framework for stability in discrete-time systems using quadratic difference forms and Lyapunov criteria. This allows for a deterministic approach to the study of stability properties of higher-order systems, and serves as a basis for the data-driven control strategy.
- As proof of concept, we carried out both simulated and experimental tests regarding control based purely on data. In all cases, we showed that a data-driven control strategy can successfully regulate a converter's output voltage even in the most complex of cases, i.e. the constant power load scenario. The theoretical material was validated with successful experimental tests, which makes them one of the most instrumental contributions in this thesis.

The theoretical framework and results presented in this thesis contribute to overcome some of the limitations imposed by model-restrictive approaches to control systems. However, the material covered here is still at an early phase in development and its research can take a considerable variety of directions. The following is a discussion of such possibilities regarding future work.

Data-driven control:

- *Different topologies.* The results developed in this thesis have been shown to successfully regulate the output of *traditional* boost converters with various dynamically complex loads. However, we are interested in observing the performance of such data-driven control strategy applied to different converter topologies controllable by linear feedback, e.g. [35] or [36]. As in the case of the boost converter, we would be interested in analyzing scenarios with increasingly complex loads, ranging from a nominal resistor to a CPL.
- *Application to other engineering branches.* We have observed that the data-driven control strategy proved to be effective in an electrical engineering context. However, there remains the question of whether such a technique is applicable to other engineering sciences that make use of control systems and dynamical representations, e.g. mechanical and/or chemical engineering.

Multi-controller approach:

- *Algorithm convergence.* The algorithm shown in Fig. 4.19 has been proven to be effective under specific initial conditions; however, we are interested in analyzing

the target LMI from an optimization standpoint in such a way that optimal initial conditions for the algorithm can be known from the start.

- *Performance conditions.* The condition established in (2.18) is entirely arbitrary; we are therefore interested in discovering whether a different set of switching thresholds and conditions affect the multi-controller's response.
- *Experimental validation of multi-controller scheme.* The multi-controller scenario was verified using PSIM, a power electronics simulator, proving to be successful in improving the converter's transient behavior. Moreover, a physical implementation using a converter prototype as well as data acquisition cards for programming would prove to be appropriate as a final validation process.

Appendix A

MATLAB Codes

A.1 Continuous-time

A.1.1 Nonlinear model solver in open loop

```
1 %%%%% This code solves the nonlinear boost converter model using the
2 %%%%% Improved-Euler numerical method. Particularly, this system is ...
   solved in
3 %%%%% open loop; no control action has been added yet.
4
5 %% Model parameters %%
6
7 E=30;      % Input voltage
8 R=100;    % Output resistance
9 C=220e-6; % Capacitance
10 L=250e-6; % Inductance
11
12 t=0;      % Initial time
13 h=1e-4;   % Integration step
14 tf=0.5;   % Final time
15 pasos=tf/h; % Total number of steps for num. method
16
17 grassgreen = 1/255*[226,20,20]; % RGB color code for plots
18
19 %% Equilibrium values %%
20
21 VC=200;   % Output voltage
22 D=(VC-E)/VC; % Duty cycle
23 IL=(1/R)*(1/(1-D))*VC; % Input current
24
25 %% Initial conditions %%
26
27 i=0;
28 v=0;
```

```
29
30
31 %%%%%%%%%%% Begin Improved Euler method %%%%%%%%%%%
32
33 for n=1:pasos
34 t(n+1)=t(n)+h;
35
36 ii=i(n);
37 vv=v(n);
38
39
40 if ii<=0
41     ii=0;
42 end
43
44 di1= E/L - (1-D)*vv/L;
45 dv1 = (1-D)*ii/C-vv/(R*C);
46
47 ii=ii+ h*di1;
48 vv=vv + h*dv1;
49
50 di2= E/L - (1-D)*vv/L;
51 dv2 = (1-D)*ii/C-vv/(R*C);
52
53 i(n+1)=i(n)+(h/2)*(di1+di2);
54 v(n+1)=v(n)+(h/2)*(dv1+dv2);
55
56
57 if i(n+1)<=0
58     i(n+1)=0;
59 end
60
61 end
62
63 %%%%%%%%%%% End Improved Euler method %%%%%%%%%%%
64
65
66 %%%%%%%%%%% Output voltage plot %%%%%%%%%%%
67
68 figure( Position , [58 327 930 378]);
69
70 subplot(1,2,1);
71 plot(t,v, LineWidth , 2)
72 title( Capacitor output voltage )
73 xlabel( Time [s] , FontSize , 12, FontWeight , bold );
74 ylabel( Output voltage [V] , FontSize , 12, FontWeight , bold );
75 xlim([0 0.25])
76 grid on
77
78 %%%%%%%%%%% Input current plot %%%%%%%%%%%
79
80 subplot(1,2,2);
```



```

39 P=sdpvar(4,4); % Unknown matrix with dimension 4 x 4
40 H=[A-k2*B*C1 -k1*B zeros(2,1);C1+g2*C2 0 g1;C2 0 0];
41 Q=transpose(H)*P+P*H; % Lyapunov criteria
42 F=[P>=0;Q<=0]; % Inequality constraints
43 solvesdp(F); % Solve inequality
44
45 P=double(P); % Save value of P, it is now known so used as input
46 k1 = sdpvar(1,1);
47 k2 = sdpvar(1,1);
48 g1 = sdpvar(1,1);
49 g2 = sdpvar(1,1); % Now, gains are unknown
50
51 H=[A-k2*B*C1 -k1*B zeros(2,1);C1+g2*C2 0 g1;C2 0 0];
52 Q=transpose(H)*P+P*H;
53 F=[Q<=0];
54
55 solvesdp(F);
56
57 k1 = double(k1);
58 cont(i,1) = k1;
59 k2 = double(k2);
60 cont(i,2) = k2;
61 g1 = double(g1);
62 cont(i,3) = g1;
63 g2 = double(g2);
64 cont(i,4) = g2; % Controller bank filling
65
66 eigv(i,:)=eig(double(H)); % Verify asymptotic stability of
67 % coefficient matrix H with obtained gains
68
69 end
70
71 %%%%%%%%%%% End BMI linearizing loop %%%%%%%%%%%
72
73
74 %%%%%% Display variables %%%%%%%
75
76 double(k1)
77 double(k2)
78 double(g1)
79 double(g2)
80 double(P)
81 1/eig(double(H))
82 cont
83 eigv

```

A.1.3 Nonlinear model solver in closed loop with multi-controller function

```

1  %%%%% This code solves the nonlinear boost converter model in closed ...
    loop.
2  %%%%% Additionally, it incorporates the multi-controller switching
3  %%%%% operation using gain sets obtained by solving the
4  %%%%% Lyapunov LMI in multiple instances.
5
6  close
7
8
9
10 %%%%%%%%%%%%%%% Model parameters %%%%%%%%%%%%%%%
11
12 E=30;      % Input voltage
13 R=100;     % Load (output) resistance
14 C=220e-6; % Capacitance
15 L=250e-6; % Inductance
16 t=0;      % Initial time
17 h=1e-06;  % Integration step
18 tf=1;     % Final time
19 pasos=tf/h; % Total number of steps for method
20
21 %%%%%%%%%%%%%%% RGB color codes for plots %%%%%%%%%%%%%%%
22
23 royalred = 1/255*[226,20,20];
24 defaultblue = [0, 0.4470, 0.7410];
25 defaultorange = [0.8500, 0.3250, 0.0980];
26
27 %% Equilibrium values %% Note: Comment following 3 lines if using
28 %% trajectory tracking.
29 VC=200;
30 D=(VC-E)/VC;
31 IL=(1/R)*(1/(1-D))*VC;
32
33 %%%%%%%%%%%%%%% Model initial conditions %%%%%%%%%%%%%%%
34
35 i=0;      % Initial current
36 v=0;      % Initial voltage
37 z=0;      % Current controller variable
38 w=0;      % Voltage controller variable
39
40 m = 0;    % Multi-controller bank index variable
41 j = 2;    % Multi-controller 5nT sampling index
42 eps = 0.1; % Multi-controller performance condition (epsilon)
43 p = size(cont,1); % Limiter variable for multicontroller re-initialization
44
45 %%%%%%%%%%%%%%% Begin model solving %%%%%%%%%%%%%%%
46
47 for n=1:pasos
48 t(n+1)=t(n)+h; % Time vector
49
50 %%%%%%%%%%%%%%% Disturbance: -20 V step in input voltage at t = 0.6 s

```

```

51
52 if n == 0.6/h
53     E = E-20;
54 end
55
56 %%%%%%%%%%%%% Disturbance: resistance decreases by half at t = 0.4 s
57
58 if n ≥ 0.4/h
59     R = R/2;
60 end
61
62
63 %%%%%%%%%%%%% Trajectory tracking %%%%%%%%%%%%%
64 % NOTE: If using this, please comment lines 29-31
65
66 % VC = 200*(1-exp(-40*t(n+1)));
67 % VC= 200*(1-exp(-20*t(n+1)).*cos(100*t(n+1)));
68 % D=(VC-E)/VC;
69 % IL=(1/R)*(1/(1-D))*VC;
70
71 %%%%%%%%%%%%% End trajectory tracking %%%%%%%%%%%%%
72
73 %%%%%%%%%%%%% Controller gains %%%%%%%%%%%%%
74
75 k1=cont(m,1);
76 k2=cont(m,2);
77 g1=cont(m,3);
78 g2=cont(m,4);
79
80 %%%%%%%%%%%%% Begin improved Euler method %%%%%%%%%%%%%
81
82 ii=i(n);
83 vv=v(n);
84 zz=z(n);
85 ww=w(n);
86
87 if ii≤0
88     ii=0; % Continuous conduction mode (CCM)
89 end
90
91 DeltaD=-[k1 k2]*[zz;ii-IL];
92 d=DeltaD+D;
93 dil=E/L - (1-d)*vv/L;
94 dvl=(1-d)*ii/C - vv/R/C;
95 dzl=ii-IL + [g1 g2]*[ww;vv-VC];
96 dwl=vv-VC - 0;
97
98 ii=ii + h*dil;
99 vv=vv + h*dvl;
100 zz=zz + h*dzl;
101 ww=ww + h*dwl;
102

```

```

103 if ii≤0
104     ii=0;
105 end
106
107 di2=E/L - (1-d)*vv/L;
108 dv2=(1-d)*ii/C - vv/R/C;
109 dz2=ii-IL + [g1 g2]*[ww;vv-VC];
110 dw2=vv-VC-0;
111
112
113 i(n+1)=i(n)+(h/2)*(di1+di2);
114 v(n+1)=v(n)+(h/2)*(dv1+dv2);
115 z(n+1)=z(n)+(h/2)*(dz1+dz2);
116 w(n+1)=w(n)+(h/2)*(dw1+dw2);
117
118 if i(n+1)≤0
119     i(n+1)=0; % Continuous conduction mode (CCM)
120 end
121
122 %%%%%%%%%%% End improved Euler method %%%%%%%%%%%
123
124 %%%%%%%%%%% Begin multi-controller function %%%%%%%%%%%
125
126 % Family of possible desired trajectories:
127
128 %trajdes(n+1) = 200*(1-exp(-40*t(n+1)));
129 %trajdes(n+1) = VC*(1-exp(-40*t(n+1)));
130 trajdes(n+1)=200*(1-exp(-40*t(n+1)).*cos(300*t(n+1)));
131
132 trajerror(n+1) = v(n+1) - trajdes(n+1); % Instantaneous error E(t)
133
134 %%%%%%%%%%% Switching condition at 5nT %%%%%%%%%%%
135
136 if n+1 == j+4
137     Δe = abs(trajerror(n+1) - trajerror(n-3));
138     if Δe > eps
139         m = m + 1;
140         disp([ Switching to row      ,num2str(m),    of controllers at ...
141              step      ,...
142              num2str(n)])
143         if m == p      % If controller bank limit has been reached
144             disp( Reinitializing controller bank... )
145             m = 1;
146         end
147     end
148     j = j + 5;
149 end
150 indice(n)=m; % Index vector for plotting
151 end
152
153 %%%%%%%%%%% End multi-controller function %%%%%%%%%%%

```

```

154
155 %%%%%%%%%%% End model solving %%%%%%%%%%%
156
157 %%%%%%%%%%% Begin plotting %%%%%%%%%%%
158
159 %%%%%%%%%%% Current -and- voltage %%%%%%%%%%%
160
161 % figure ( Position , [58 327 930 378] );
162 %
163 %
164 % subplot(1,2,1);
165 % plot(t,v, LineWidth,2)
166 % title( Capacitor output voltage )
167 % xlabel( Time [s] , FontSize , 12, FontWeight , bold );
168 % ylabel( Output voltage [V] , FontSize , 12, FontWeight , bold );
169 % grid on
170 %
171 %
172 %
173 % subplot(1,2,2);
174 % plot(t,i, Color , royalred, linewidth,2)
175 % title( Inductor input current )
176 % xlabel( Time [s] , FontSize , 12, FontWeight , bold );
177 % ylabel( Input current [A] , FontSize , 12, FontWeight , bold );
178 % ylim([0 30])
179 % grid on
180
181
182 %%%%%%%%%%% Plot voltage and desired trajectories %%%%%%%%%%%
183
184 figure( Position , [193 188 630 378] );
185 hold on
186 plot(t,trajdes, LineWidth ,1.5, DisplayName , Desired trajectory ,...
187      Color , defaultorange)
188 plot(t,v, LineWidth ,1.5, DisplayName , Output ...
189      voltage , Color ,defaultblue)
189 xlim([0 tf])
190 title( Multi-controller system performance, ? = 0.1 )
191 xlabel( Time [s] , FontSize , 12, FontWeight , bold );
192 ylabel( Voltage [V] , FontSize , 12, FontWeight , bold );
193 grid on
194 legend( location , southeast )
195
196
197 %%%%%%%%%%% End plotting %%%%%%%%%%%

```

A.2 Discrete-time

A.2.1 Data extractor: Importing data from .txt file to MATLAB and reducing its integration step

```

1  %%%% This code is used for data-driven control purposes; first, given a
2  %%%% set of data corresponding to variable measurements, this code ...
   reduces
3  %%%% their integration step to any arbitrary number for ease of
4  %%%% implementation in numerical computations.
5
6  %%%% Second, this code calculates the -error variables- by subtracting
7  %%%% their value from a desired equilibrium.
8
9  %%%% This algorithm assumes that data are given in a matrix
10 %%%% formed by -column vectors-.
11
12
13 %%%%%%%%%%%%%%% Data reading %%%%%%%%%%%%%%%
14
15 M = dlmread( 'datos.txt' ); % This command accepts a .txt file containing
16 % the data (note: there must be NO text inside the file for this to work)
17 v = M(:,2); % In .txt file, column 2 corresponds to voltage data
18 d = M(:,3); % In .txt file, column 3 corresponds to duty cycle data
19 i = M(:,4); % In .txt file, column 4 corresponds to current data
20
21 %%%%%%%%%%% Equilibrium values %%%%%%%%%%%
22
23 V = 100; % Voltage
24 D = 0.5; % Duty cycle
25 I = 4;   % Current
26
27 %%%%%%%%%%% Creation of error variables %%%%%%%%%%%
28
29  $\Delta v = v - V;$ 
30  $\Delta d = d - D;$ 
31  $\Delta i = i - I;$ 
32
33 %%%%%%%%%%% Transposing data to make them -row vectors- %%%%%%%%%%%
34
35  $\Delta v = \text{transpose}(\Delta v);$ 
36  $\Delta d = \text{transpose}(\Delta d);$ 
37  $\Delta i = \text{transpose}(\Delta i);$ 
38
39 %%%%%%%%%%% Creation of new, smaller vectors %%%%%%%%%%%
40
41  $\Delta v_f = \Delta v(:,1);$ 
42  $\Delta d_f = \Delta d(:,1);$ 
43  $\Delta i_f = \Delta i(:,1);$ 

```

```

44
45 %%%%%%%%% Time step reduction %%%%%%%%%
46
47 paso = 100; % Define number by which to divide original integration step
48
49 k=2;
50 for j=paso:paso:size(M,1)
51     Δvf(:,k) = Δv(:,j);
52     k=k+1;
53 end
54
55 k=2;
56 for j=paso:paso:size(M,1)
57     Δdf(:,k) = Δd(:,j);
58     k=k+1;
59 end
60
61
62 k=2;
63 for j=paso:paso:size(M,1)
64     Δi_f(:,k) = Δi(:,j);
65     k=k+1;
66 end
67
68
69 w = [Δdf;Δi_f;Δvf]; % Algorithm output: Data matrix w of the form
70 % w(t) = [Δ.D(t);Δ.i(t);Δ.v(t)], one set for each step (t)
71 % Note: The resulting time series / data matrix can be used in the
72 % calculation of -Hankel matrices- for data-driven control purposes.

```

A.2.2 Hankel matrix builder from data set in time-series form: Lag 1

```

1 %%%%%%%%% This code is used to construct a Hankel matrix of depth 2 from ...
   a congruently
2 %%%%%%%%% partitioned set of data. This code admits a previously obtained ...
   data set
3 %%%%%%%%% labeled as w. The output is therefore coefficient matrices R0 and
4 %%%%%%%%% R1.
5
6
7 N = 1 ; % Lag (Max. derivative coefficient)
8 L = N + 1; % Depth of Hankel matrix
9 T = size(w,2); % Length of time series
10
11 %%%%%%%%% Build Hankel matrix in form of cell array %%%%%%%%%
12
13 for i=1:L
14     for j=1:T-L+1

```



```

15         H{i, j} = w(:, j+i-1);
16     end
17 end
18
19 H2 = cell2mat(H); % Converts cell array to matrix
20
21 [U,S,V] = svd(H2); % Perform singular value decomposition of Hankel matrix
22
23 %%%%%%%%%% Apply system identification theory %%%%%%%%%%
24
25 u2 = [U(:,5) U(:,6)]; % Number of columns in u2 is equal to number of ...
    outputs
26 R = transpose(u2);
27 R0 = [R(:,1) R(:,2) R(:,3)]
28 R1 = [R(:,4) R(:,5) R(:,6)]

```

A.2.3 Hankel matrix builder from data set in time-series form: Lag 2

```

1 %%%%%%%%% This code is used to construct a Hankel matrix of depth 2 from ...
    a congruently
2 %%%%%%%%% partitioned set of data. This code admits a previously obtained ...
    data set
3 %%%%%%%%% labeled as w. The output is therefore coefficient matrices R0,
4 %%%%%%%%% R1 and R2.
5
6
7 N = 2 ; % Lag (Max. derivative coefficient)
8 L = N + 1; % Depth of Hankel matrix
9 T = size(w,2); % Length of time series
10
11 %%%%%%%%% Build Hankel matrix in form of cell array %%%%%%%%%
12
13 for i=1:L
14     for j=1:T-L+1
15         H{i, j} = w(:, j+i-1);
16     end
17 end
18
19 H2 = cell2mat(H); % Converts cell array to matrix
20
21 [U,S,V] = svd(H2); % Perform singular value decomposition of Hankel matrix
22
23 %%%%%%%%% Apply system identification theory %%%%%%%%%
24
25 u2 = [U(:,5) U(:,6)]; % Number of columns in u2 is equal to number of ...
    outputs
26 R = transpose(u2);
27 R0 = [R(:,1) R(:,2) R(:,3)]

```

```

28 R1 = [R(:,4) R(:,5) R(:,6)]
29 R2 = [R(:,7) R(:,8) R(:,9)]

```

A.2.4 Discrete-time control: Gain computation by Lyapunov LMI solving (LDS of lag 1)

```

1
2 %%%%% This code solves the higher-order discrete-time Lyapunov LMI
3 %%%%% multiple times, using coefficient matrices built via Hankel matrix
4 %%%%% SVD in conjunction with discrete-time linear controllers.
5 %%%%% The output of interest in this algorithm are gain values
6 %%%%% k1, k2, g1, g2.
7
8 close
9 clc
10
11 N = 1; % Maximum lag in linear difference system
12 q = 5; % Size of augmented external variable vector
13
14 % Controller gains: Initial conditions (Very close to zero)
15 % Note: Can be whatever is expected to converge optimally
16
17 k1 = 0.001;
18 k2 = 0.001;
19 g1 = 0.001;
20 g2 = 0.01;
21
22 pasos = 50; % Number of times LMI will be solved
23 cont = zeros(pasos,4); % Controller bank array definition
24
25 %%%%%%%%%%%%% Begin BMI linearizing loop %%%%%%%%%%%%%
26
27 for i=1:pasos
28
29     Y=sdpvar(q, (N+1)*q); % Unknown matrix with accurate dimensions
30     K = sdpvar(N*q,N*q); % Coefficient matrix that ensures stability
31     R = [R0 zeros(size(R0,1),1) zeros(size(R0,1),1) R1 ...
32         zeros(size(R1,1),1)...
33         zeros(size(R1,1),1);
34         1 k2*[1 0] k1 0 0 0 0 0 0;
35         0 -[1 g2] -1 -g1 0 0 0 1 0;
36         0 0 -1 0 -1 0 0 0 0 1]; % Augmented coefficient matrix
37     Q = [zeros(q,q) zeros(q,N*q); zeros(N*q,q) K] - [K zeros(N*q,N*q);...
38         zeros(q,N*q) zeros(q,q)] + R * Y + Y * R; % Stability condition
39
40     F=[Q<=0;K>=0]; % Inequality constraints
41     solvesdp(F); % Solve inequality

```

```

42
43     Y = double(Y); % Save value of Y; now serves as input
44     K = sdpvar(N*q,N*q);
45     k1 = sdpvar(1,1);
46     k2 = sdpvar(1,1);
47     g1 = sdpvar(1,1);
48     g2 = sdpvar(1,1); % Gains are now unknown
49
50     R = [R0 zeros(size(R0,1),1) zeros(size(R0,1),1) R1 ...
zeros(size(R1,1),1)...
51         zeros(size(R1,1),1);
52         1 k2*[1 0] k1 0 0 0 0 0 0;
53         0 -[1 g2] -1 -g1 0 0 0 1 0;
54         0 0 -1 0 -1 0 0 0 0 1];
55     Q = [zeros(q,q) zeros(q,N*q); zeros(N*q,q) K] - [K zeros(N*q,N*q);...
56         zeros(q,N*q) zeros(q,q)] + R * Y + Y * R;
57
58     F=[Q<=0;K>=0];
59     solvesdp(F); % Solve inequality once more
60
61     k1 = double(k1);
62     cont(i,1) = k1;
63     k2 = double(k2);
64     cont(i,2) = k2;
65     g1 = double(g1);
66     cont(i,3) = g1;
67     g2 = double(g2);
68     cont(i,4) = g2; % Controller bank filling
69
70 end
71
72 %%%%%%%%%%% End BMI linearizing loop %%%%%%%%%%%

```

A.2.5 Discrete-time control: Gain computation by Lyapunov LMI solving (LDS of lag 2)

```

1  %%%% This code solves the higher-order Lyapunov inequality for a linear
2  %%%% difference system of lag 2. Code functionality is exactly the same
3  %%%% as the lag 1 version; only coefficient matrices and dimensions
4  %%%% change between versions.
5
6  clc
7  close
8
9  L = 2; % Maximum lag in linear difference system
10 w = 5; % Size of augmented external variable vector
11
12

```

```

13 % Controller gains: Initial conditions (Very close to zero)
14 % Note: Can be whatever is expected to converge optimally
15
16 k1 = 0.001;
17 k2 = 0.001;
18 g1 = 0.001;
19 g2 = 0.01;
20
21 %%%%%%%%%%%
22
23 pasofinal = 50; % Number of times LMI will be solved
24 cont = zeros(pasofinal,4); % Controller bank array definition
25
26 %%%%%%%%%%% Begin BMI linearizing loop %%%%%%%%%%%
27
28 for i=1:pasofinal
29
30 Y=sdpvar(w, (L+1)*w); % Unknown matrix with accurate dimensions
31 Psi = sdpvar(L*w,L*w); % Coefficient matrix that ensures stability
32 P = [1 k2*[1 0] k1 0 0 0 0 0 0 zeros(1,5); R0 zeros(2,2) R1 zeros(2,2)...
33      R2 zeros(2,2); 0 -[1 g2] -1 -g1 0 0 0 1 0 zeros(1,5); ...
34      0 -[0 1] 0 -1 0 0 0 0 1 zeros(1,5)]; % Augmented coeff. matrix
35 Q1=[zeros(w,w) zeros(w,L*w); zeros(L*w,w) Psi]-[Psi zeros(L*w,w);...
36      zeros(w,L*w) zeros(w,w)]+Y *P+P *Y; % Stability condition
37 F=[Q1<=0;Psi>=0]; % Inequality constraints
38 solvesdp(F); % Solve the LMI
39
40
41 Y=double(Y); % Save value of Y; now serves as input
42 Psi = sdpvar(L*w,L*w); % Calculate to ensure stability
43 k1 = sdpvar(1,1)
44 k2 = sdpvar(1,1);
45 g1 = sdpvar(1,1);
46 g2 = sdpvar(1,1); % Gains are now unknown
47
48 P = [1 k2*[1 0] k1 0 0 0 0 0 0 zeros(1,5); R0 zeros(2,2) R1 zeros(2,2)...
49      R2 zeros(2,2); 0 -[1 g2] -1 -g1 0 0 0 1 0 zeros(1,5);...
50      0 -[0 1] 0 -1 0 0 0 0 1 zeros(1,5)];
51 Q2=[zeros(w,w) zeros(w,L*w); zeros(L*w,w) Psi]-[Psi zeros(L*w,w);...
52      zeros(w,L*w) zeros(w,w)]+Y *P+P *Y;
53 F=[Q2<=0;Psi>=0;]; % Solve inequality once more
54 solvesdp(F);
55
56
57 k1 = double(k1);
58 cont(i,1) = k1;
59 k2 = double(k2);
60 cont(i,2) = k2;
61 g1 = double(g1);
62 cont(i,3) = g1;
63 g2 = double(g2);
64 cont(i,4) = g2; % Controller bank filling

```

```

65
66 end
67
68 %%%%%%%%%%% End BMI linearizing loop %%%%%%%%%%%

```

A.2.6 Linearized model solver in closed loop

```

1 %%%%%% This code solves the linearized boost converter model in
2 %%%%%% closed-loop. Two controllers are used: one for current and another
3 %%%%%% one for voltage. This code is useful for verifying whether or ...
   not a
4 %%%%%% certain gain set is able to stabilize the model at the origin, i.e.
5 %%%%%% it abides by Lyapunov stability theory. Note that the Improved ...
   Euler
6 %%%%%% method is applied.
7
8 %%%%%%%%%%% Model parameters %%%%%%%%%%%
9
10 E=30;      % Input voltage
11 R=100;     % Load (output) resistance
12 C=220e-6; % Capacitance
13 L=250e-6; % Inductance
14 t=0;      % Initial time
15 h=1e-04;  % Integration step
16 tf=1;     % Final time
17 pasos=tf/h; % Total number of steps for method
18
19
20 %%%%%%%%%%% Model coefficient matrices %%%%%%%%%%%
21 % These are a discretized version of the linearized state-space ...
   coefficient
22 % matrices A and B. These are obtained by means of the c2d command.
23
24 A= [0.998 -0.05982; 0.06798 0.9934];
25 B= [80.13;-3.321];
26
27 %%%%%%%%%%% Model initial conditions %%%%%%%%%%%
28
29 i=-20; % Initial current (Arbitrary)
30 v=-15; % Initial voltage (Arbitrary)
31 z=0; % Current controller variable z
32 w=0; % Voltage controller variable w
33 x=[i v] ; % State vector definition
34
35 %%%%%%%%%%% Controller gains (Obtained via Lyapunov LMI) ...
   %%%%%%%%%%%
36
37 k1 = 0.0060;

```

```

38 k2 = 0.0152;
39 g1 = 0.0544;
40 g2 = 0.5730;
41
42 %%%%%%%%% Ciclo de soluci n %%%%%%%%%
43
44
45 for n=1:pasos
46     t(n+1) = t(n)+h; % Time vector, used in plots
47     x(:,n+1) = A*x(:,n)+B*(-k1*z(n)-k2*[1 0]*x(:,n));
48     z(n+1) = z(n)+[1 0]*x(:,n)+g1*w(n)+g2*[0 1]*x(:,n);
49     w(n+1) = w(n)+[0 1]*x(:,n); % Model / controller equations
50 end
51
52 %%%%%%%%% Output voltage plot %%%%%%%%%
53
54 figure( Position , [58 327 930 378]);
55
56 plot(t,x(1,:), LineWidth ,2)
57 title( Capacitor output voltage )
58 xlabel( Time [s] , FontSize , 12, FontWeight , bold );
59 ylabel( Output voltage [V] , FontSize , 12, FontWeight , bold );
60 xlim([0 tf])
61 grid on

```

Remark A.1. For a downloadable version of the previously presented codes, please refer to the following link: <https://tinyurl.com/y3tkqcon>.

Bibliography

- [1] D. Liberzon. *Switching in Systems and Control*. Birkhauser. Boston, Basel, Berlin, 2003.
- [2] M. Su, Z. Liu, Y. Sun, H. Han, and X. Hou. Stability analysis and stabilization methods of dc microgrid with multiple parallel-connected DC-DC converters loaded by cpls. *IEEE Transactions on Smart Grid*, 9(1):132–142, Jan 2018. ISSN 1949-3053. doi: 10.1109/TSG.2016.2546551.
- [3] Y. Gu, W. Li, and X. He. Passivity-based control of dc microgrid for self-disciplined stabilization. *IEEE Transactions on Power Systems*, 30(5):2623–2632, Sept 2015. ISSN 0885-8950. doi: 10.1109/TPWRS.2014.2360300.
- [4] M. Karbalaye Zadeh, R. Gavagsaz-Ghoachani, S. Pierfederici, B. Nahid-Mobarakeh, and M. Molinas. Stability analysis and dynamic performance evaluation of a power electronics-based dc distribution system with active stabilizer. *IEEE Journal of Emerging and Selected Topics in Power Electronics*, 4(1):93–102, March 2016. ISSN 2168-6777. doi: 10.1109/JESTPE.2015.2484218.
- [5] Jianwu Zeng, Zhe Zhang, and Wei Qiao. An interconnection and damping assignment passivity-based controller for a DC-DC boost converter with a constant power load. *IEEE Trans. Ind. Applic.*, 50(4):2314–2322, July. 2014. ISSN 0093-9994. doi: 10.1109/TIA.2013.2290872.
- [6] Q. Xu, C. Zhang, C. Wen, and P. Wang. A novel composite nonlinear controller for stabilization of constant power load in dc microgrid. *IEEE Transactions on Smart Grid (In press)*, 2017. ISSN 1949-3053. doi: 10.1109/TSG.2017.2751755.
- [7] Y. Huangfu, S. Pang, B. Nahid-Mobarakeh, L. Guo, A. K. Rathore, and F. Gao. Stability analysis and active stabilization of on-board dc power converter system with input filter. *IEEE Transactions on Industrial Electronics*, 65(1):790–799, Jan 2018. ISSN 0278-0046. doi: 10.1109/TIE.2017.2703663.
- [8] L. M. Saublet, R. Gavagsaz-Ghoachani, J. P. Martin, B. Nahid-Mobarakeh, and S. Pierfederici. Asymptotic stability analysis of the limit cycle of a cascaded DC-DC converter using sampled discrete-time modeling. *IEEE Trans. Ind. Electr.*, 63(4):2477–2487, April 2016. ISSN 0278-0046. doi: 10.1109/TIE.2015.2509908.

- [9] L. Fangcheng, L. Jinjun, Z. Haodong, and X. Danhong. Stability issues of $Z + Z$ type cascade system in hybrid energy storage system (HESS). *IEEE Trans. Power Electr.*, 29(11):5846–5859, Nov. 2014. ISSN 0885-8993. doi: 10.1109/TPEL.2013.2295259.
- [10] B. H. Kim and S. K. Sul. Shaping of pwm converter admittance for stabilizing local electric power systems. *IEEE Journal of Emerging and Selected Topics in Power Electronics*, 4(4):1452–1461, Dec 2016. ISSN 2168-6777. doi: 10.1109/JESTPE.2016.2594041.
- [11] A. Aldhaheri and A. H. Etemadi. Stabilization and performance preservation of dc-dc cascaded systems by diminishing output impedance magnitude. *IEEE Transactions on Industry Applications (In press)*, 2017. ISSN 0093-9994. doi: 10.1109/TIA.2017.2766045.
- [12] M. Hamzeh, M. Ghafouri, H. Karimi, K. Sheshyekani, and J. M. Guerrero. Power oscillations damping in dc microgrids. *IEEE Transactions on Energy Conversion*, 31(3):970–980, Sept 2016. ISSN 0885-8969. doi: 10.1109/TEC.2016.2542266.
- [13] X. Lu, K. Sun, J. M. Guerrero, J. C. Vasquez, L. Huang, and J. Wang. Stability enhancement based on virtual impedance for dc microgrids with constant power loads. *IEEE Transactions on Smart Grid*, 6(6):2770–2783, Nov 2015. ISSN 1949-3053. doi: 10.1109/TSG.2015.2455017.
- [14] L. Guo, S. Zhang, X. Li, Y. W. Li, C. Wang, and Y. Feng. Stability analysis and damping enhancement based on frequency-dependent virtual impedance for dc microgrids. *IEEE Journal of Emerging and Selected Topics in Power Electronics*, 5(1):338–350, March 2017. ISSN 2168-6777. doi: 10.1109/JESTPE.2016.2598821.
- [15] M. Zhang, Y. Li, F. Liu, L. Luo, Y. Cao, and M. Shahidehpour. Voltage stability analysis and sliding-mode control method for rectifier in dc systems with constant power loads. *IEEE Journal of Emerging and Selected Topics in Power Electronics*, 5(4):1621–1630, Dec 2017. ISSN 2168-6777. doi: 10.1109/JESTPE.2017.2723482.
- [16] M. Wu and D. D. C. Lu. A novel stabilization method of lc input filter with constant power loads without load performance compromise in dc microgrids. *IEEE Trans. Ind. Electr.*, 62(7):4552–4562, July 2015. ISSN 0278-0046. doi: 10.1109/TIE.2014.2367005.
- [17] Jonathan C. Mayo-Maldonado. *Switched linear differential systems*. PhD thesis, 2015.
- [18] Y. Xinghuo, C. Cecati, T. Dillon, and M.G. Simes. The new frontier of smart grids. *IEEE Ind. Electr. Mag.*, 5(3):49–63, Sept. 2011. ISSN 1932-4529. doi: 10.1109/MIE.2011.942176.

- [19] H. Zhang, J. Zhou, Q. Sun, J. M. Guerrero, and D. Ma. Data-driven control for interlinked ac/dc microgrids via model-free adaptive control and dual-droop control. *IEEE Transactions on Smart Grid*, 8(2):557–571, March 2017. ISSN 1949-3053. doi: 10.1109/TSG.2015.2500269.
- [20] S. A. Hashjin and B. Nahid-Mobarakeh. Active stabilization of a microgrid using model free adaptive control. In *2017 IEEE Industry Applications Society Annual Meeting*, pages 1–8, Oct 2017. doi: 10.1109/IAS.2017.8101797.
- [21] L. Herrera, W. Zhang, and J. Wang. Stability analysis and controller design of dc microgrids with constant power loads. *IEEE Transactions on Smart Grid*, 8(2): 881–888, March 2017. ISSN 1949-3053. doi: 10.1109/TSG.2015.2457909.
- [22] M. Kabalan, P. Singh, and D. Niebur. Large signal lyapunov-based stability studies in microgrids: A review. *IEEE Transactions on Smart Grid*, 8(5):2287–2295, Sept 2017. ISSN 1949-3053. doi: 10.1109/TSG.2016.2521652.
- [23] H. Mosskull. Optimal dc-link stabilization design. *IEEE Trans. Ind. Electr.*, 62(8): 5031–5044, Aug 2015. ISSN 0278-0046. doi: 10.1109/TIE.2015.2397872.
- [24] T. Xisheng, D. Wei, and Q. Zhiping. Investigation of the dynamic stability of microgrid. *IEEE Trans. Power Syst.*, 29(2):698–706, Mar. 2014. ISSN 0885-8950. doi: 10.1109/TPWRS.2013.2285585.
- [25] F. Golnaraghi and B. C. Kuo. *Automatic control systems*. John Wiley Sons, 2010.
- [26] Hassan K. Khalil. *Nonlinear systems*. Pearson Education International Inc., 2015.
- [27] J. Lofberg. Yalmip : a toolbox for modeling and optimization in matlab. In *2004 IEEE International Conference on Robotics and Automation (IEEE Cat. No.04CH37508)*, pages 284–289, Sep. 2004. doi: 10.1109/CACSD.2004.1393890.
- [28] H. Sira-Ramírez and R. Silva-Ortigoza. *Control design techniques in power electronics devices*. Springer, 2006.
- [29] C. Moo and G. Wu. Maximum power point tracking with ripple current orientation for photovoltaic applications. *IEEE Journal of Emerging and Selected Topics in Power Electronics*, 2(4):842–848, Dec 2014. ISSN 2168-6777. doi: 10.1109/JESTPE.2014.2328577.
- [30] P. F. Miaja, M. Rodriguez, A. Rodriguez, and J. Sebastian. A linear assisted dc/dc converter for envelope tracking and envelope elimination and restoration applications. *IEEE Transactions on Power Electronics*, 27(7):3302–3309, July 2012. ISSN 0885-8993. doi: 10.1109/TPEL.2011.2181869.
- [31] H. Lin and P. J. Antsaklis. Stability and stabilizability of switched linear systems: A survey of recent results. *IEEE Transactions on Automatic Control*, 54(2):308–322, Feb 2009. ISSN 0018-9286. doi: 10.1109/TAC.2008.2012009.

-
- [32] C. Kojima and K. Takaba. A generalized lyapunov stability theorem for discrete-time systems based on quadratic difference forms. *Proceedings of the 44th IEEE Conference on Decision and Control*. doi: 10.1109/cdc.2005.1582606.
- [33] T.M. Maupong and P. Rapisarda. Data-driven control: A behavioral approach. *Systems & Control Letters*, 101:37–43, 2017. ISSN 01676911. doi: 10.1016/j.sysconle.2016.04.006.
- [34] Ernesto Salas-Esquivel. Data-Driven Approach to Topology Change Location in Distribution Networks Using μ PMUs. Master’s thesis, Tecnológico de Monterrey, Monterrey, Mexico, 2018.
- [35] P. M. Garcia-Vite, J. E. Valdez-Resendiz, J. C. Mayo-Maldonado, J. C. Rosas-Caro, M. del Rosario Rivera-Espinosa, and A. Valderrabano-Gonzalez. Quadratic gain converter with output voltage ripple mitigation. In *2017 IEEE Energy Conversion Congress and Exposition (ECCE)*, pages 2253–2259, Oct 2017. doi: 10.1109/ECCE.2017.8096439.
- [36] J. C. Mayo-Maldonado, J. E. Valdez-Resendiz, P. M. Garcia-Vite, J. C. Rosas-Caro, M. del Rosario Rivera-Espinosa, and A. Valderrabano-Gonzalez. Quadratic buckboost converter with zero output voltage ripple at a selectable operating point. *IEEE Transactions on Industry Applications*, 55(3):2813–2822, May 2019. ISSN 0093-9994. doi: 10.1109/TIA.2018.2889421.